Development and application of an alternative modelling approach for the thermo-mechanical analysis of a DEMO Water-Cooled Lithium Lead breeding blanket segment

Ilenia Catanzaro[a]*, Gaetano Bongiovì[a], Pierluigi Chiovaro[a], Pietro Alessandro Di Maio[a], Gandolfo Alessandro Spagnuolo[b]

[a] *Università degli Studi di Palermo, Dipartimento di Ingegneria, Viale delle Scienze, Edificio 6, 90128 Palermo, ITALY*

[b] *EUROfusion Consortium, Programme Management Unit, Garching, GERMANY*

In the frame of the EUROfusion research activities devoted to the design of the DEMO breeding blanket (BB), the Water-Cooled Lithium-Lead BB (WCLL) concept is one of the candidates currently assessed in EU. To this end, an intense research campaign is ongoing to develop a robust geometric configuration for the WCLL BB Central Outboard Segment (COB). Since the current reference design of the WCLL COB segment is not mature enough to allow a full thermal-hydraulic assessment, an alternative procedure aimed at obtaining a thermal field for the whole segment without performing its complete thermal-hydraulic analysis is presented and applied in this work. The scope of the work is to obtain a thermal field for the whole WCLL COB segment detailed enough to ensure a reliable prediction of the secondary stress spatial distribution, which is pivotal for the segment structural analysis.

The procedure is articulated in three steps. Firstly, a thermal analysis of the equatorial region of the WCLL COB is performed, in order to calculate the thermal field in the most loaded region of the segment. Then, a multi-region interpolation is carried out in order to obtain a set of polynomial functions of the radial and toroidal variable, accurately representing the thermal field of the assessed equatorial BB slice. Finally, the calculated functions are applied to the whole COB to impose a realistic thermal field to the segment for the prediction of the stress, strain and displacement fields.

Since the mesh for the analysis of the whole segment is expected to be coarser than that used for the assessment of its equatorial region, in this paper a mesh independence assessment of the interpolating functions is reported. In particular, their predictive power both in terms of temperature and secondary stress (i. e. thermal-induced stress) is assessed taking into account a decreasing level of detail of the adopted spatial discretization grid.

The obtained results, widely reported and discussed hereafter together with the models and the adopted assumptions, show a great predictive power of the adopted polynomial functions, with a good mesh independence of the calculated temperature and stress values.

Keywords: WCLL BB; thermo-mechanics; COB segment; analysis procedure; secondary stress.

**corresponding author's email: ilenia.catanzaro@unipa.it*

1. Introduction

In the framework of the research activities fostered by the EUROfusion consortium [1], the development of a robust breeding blanket system (BB) is crucial for the design of the whole DEMO reactor [2][3]. To this goal, the thermo-mechanical assessment of the whole BB segments is necessary to allow checking the segments' structural performances against the RCC-MRx design rules, either in nominal and in accidental loading scenario. In this regard, the prediction of a realistic and accurate thermal field for the considered BB segments is pivotal to perform detailed enough thermo-mechanical analysis. In fact, from the structural assessments performed during the DEMO BB pre-conceptual phase [4], emerged that the thermal-induced stress (i. e. the secondary stress) is the main responsible of the failure in the RCC-MRx rules verification. Nevertheless, the full thermal assessment of a whole BB segment requires, firstly, the detailed knowledge of its cooling system layout. Seeing as the current design of the DEMO Water Cooled Lithium Lead (WCLL) BB is not mature enough to allow such a kind of assessment, which would require, in any case, a considerable modelling effort as well as a huge computational burden [5], assumptions and alternative models are necessary to realistically predict the thermal field of a whole WCLL BB segment. Hence, the development of alternative calculation procedures capable of predicting a realistic thermal field for a whole BB segment, without the necessity to directly perform the full thermal analysis of the whole component, can represent an important outcome. Especially in case where the design by analysis strategy is followed, a procedure allowing to easily obtain a realistic and detailed thermal field for the whole BB segment without performing thermal-hydraulic analysis could be helpful to speed up the design. In fact, such a kind of procedure can allow selecting, among a wide range of solutions, the most promising configurations to be studied, in a second step, with dedicated thermal-hydraulic assessments.

Then, in this paper, a procedure to obtain a realistic thermal field for the Central Outboard Blanket (COB) segment of the DEMO WCLL BB, starting from the thermal analysis of its equatorial region, is presented. First, a thermal analysis of the COB segment's equatorial region has been performed under nominal conditions to calculate the corresponding thermal field. To this end, the WCLL2019.v06 geometric layout has been adopted for the equatorial region modelling [6]. Then, a set of polynomial functions of the radial and toroidal variables has been selected in order to interpolate the calculated thermal field and to realistically predict the corresponding secondary stress field. After that, a mesh independence study has been performed in order to assess the applicability of the found interpolation strategy to coarser mesh, in sight of their use to impose a thermal field to the whole segment. Indeed, in order to save computational resources and time, usually the whole segment is discretized with a lower level of detail with respect to a model reproducing only a local region. Results have allowed concluding a substantial mesh independence of the proposed interpolation procedure, with positive outcomes in sigh of its application for the prediction of a realistic thermal field, and of the consequent secondary stress field, within the whole WCLL COB segment. Then, in the end, the found set of interpolation functions has been used to impose a thermal field the WCLL COB segment in order to calculate its secondary stress spatial distribution.

2. Thermal analysis of the WCLL COB segment equatorial region

In order to obtain a reliable interpolation procedure for the thermal field of the WCLL COB segment, the first step has consisted in the thermal analysis of the most loaded region, namely its equatorial

region, under steady state nominal loading conditions. To this purpose, a dedicated FEM model has been set-up and the corresponding analysis has been carried out.

2.1 The FEM model

A detailed FEM model reproducing the equatorial region of the reference WCLL2019 COB geometric configuration has been set-up, considering the v06 geometric layout [6]. Figure 1 shows the whole model, including the Segment Box (SB) composed by the First Wall (FW), the Side Walls (SWs), the internal Stiffening Plates (SPs), the Back-Plates (BPs) and the Back Supporting Structures (BSS). The SB is depicted in Figure 1 in two different colours, grey for the structural material Eurofer and green for the Tungsten armour. Moreover, the Double Walled Tubes (DWTs) are reported in blue whereas the PbLi (i. e. the breeder) in yellow. In particular this model is characterized by a thickness of horizontal and vertical SPs equal to 10 mm and 12 mm, respectively, and is endowed with the DWTs layout, reported in Figure 1, which foreseen 22 tubes in each poloidal slice. Moreover, each slice is endowed with a 10 channel FW, as shown in Figure 1.

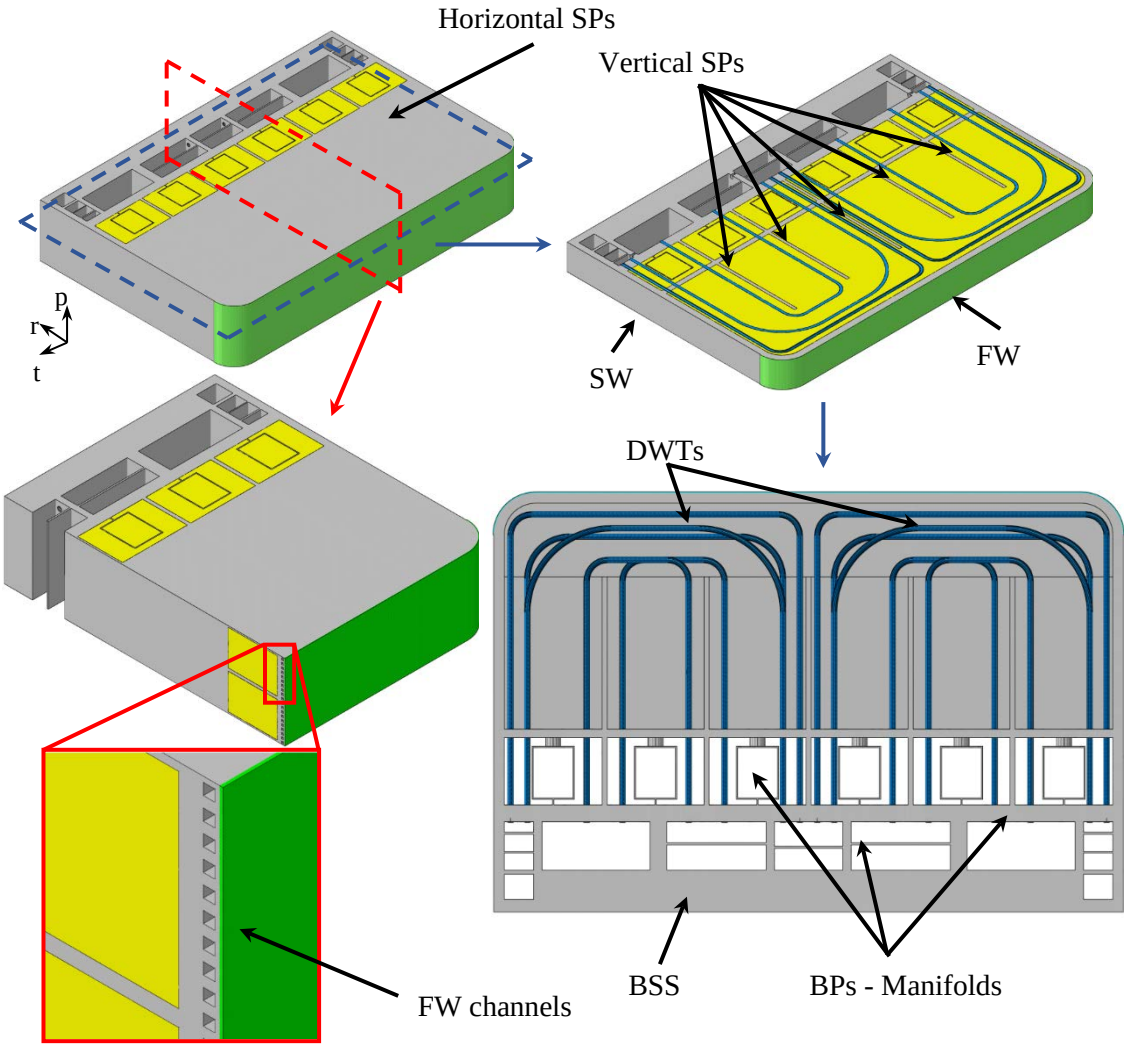

Figure 1. The WCLL2019.v06 geometric layout [6].

A mesh composed of ~2.5M nodes connected in ~2.7M hexahedral and tetrahedral linear elements has been set up for this geometric model. Temperature-dependent thermo-physical properties for Eurofer, Pb-15.7Li and Tungsten have been drawn from [7][8] and [9], respectively.

In order to predict the steady state thermal response of the assessed WCLL COB equatorial region, the following set of loads and boundary conditions has been imposed:

- non-uniform heat flux onto the tungsten armour's plasma facing surface, characterised by a maximum value of 0.32 W/m^2 [10];
- non-uniform volumetric density of nuclear heat power, calculated in-house at the University of Palermo by means a fully heterogenous neutronic model (Figure 2);
- forced convective heat transfer onto water-wetted surfaces, simulated by imposing a boundary condition characterized by a sink temperature of 311.5 °C (the average between the inlet and outlet coolant temperature [6]) and a uniform convective heat transfer coefficient purposely calculated by means of the Dittus&Bölter correlation;
- water manifolds surfaces temperature equal to 311.5 °C;
- thermal contact model between breeder and steel characterized by a thermal conductance of 100 kW/m² °C [6]
- thermal coupling between the radial-toroidal upper face and the radial-toroidal lower face.

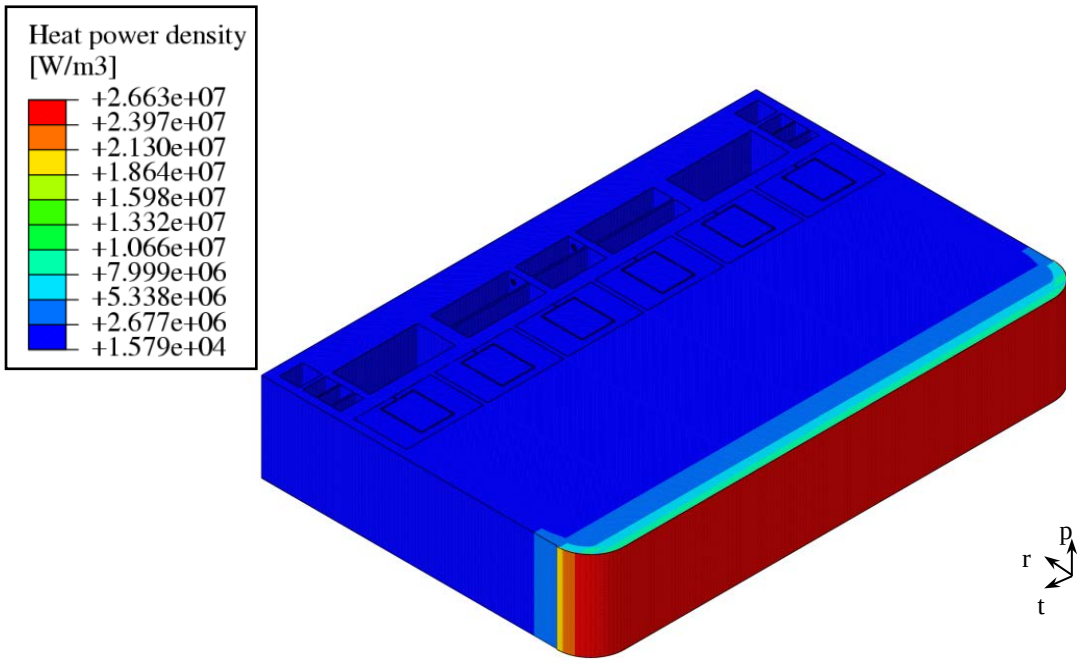

Figure 2. The volumetric density of nuclear heat power field calculated in-house.

2.2 Results

Adopting the FEM model described above, steady state thermal analysis has been performed. Results have shown that temperature values predicted within the SB remain below the Eurofer maximum allowable value of 550 °C, and the maximum value is reached within the horizontal SPs, as shown in Figure 3.

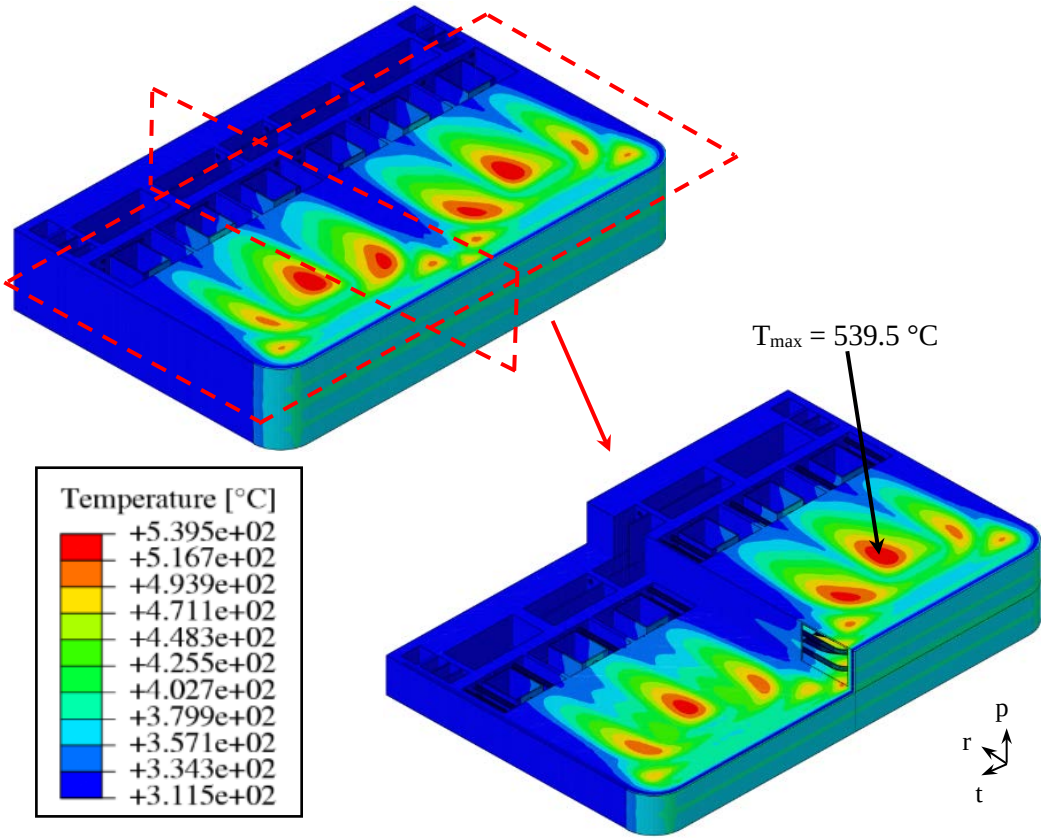

Figure 3. Thermal field arising within the SB.

3. Interpolation of the calculated thermal field

Once calculated the thermal field arising within the equatorial region of the WCLL COB SB, its exportation to the whole segment is not straightforward. Hence, observing that the thermal field calculated within the equatorial region mainly depends on radial and toroidal variables, an interpolation procedure has been performed to attain a set of polynomial functions capable of best reproducing it. Then, in order to introduce the dependence on the poloidal variable so to apply the thermal field to the whole segment, a user subroutine has been properly set-up using the Fortran programming language.

To this end, after several attempts, a "multi-region" interpolation strategy has been pursued, dividing the assessed domain in several regions: SW-FW-SW region (in green in Figure 4), 6 different regions for the toroidal-radial (i. e. horizontal) SPs (in grey in Figure 4, each delimited by a vertical SP), 5 different regions for the vertical SPs (in blue in Figure 4) and, lastly, a manifolds region (in orange in Figure 4). Hence, in total, the calculation domain has been divided in 13 different regions and a polynomial function of one or two variables (i. e. radial and toroidal variables) has been searched for each region in order to best reproduce the original thermal field:

- SW-FW-SW region: 14^{th} degree polynomial function of two variables (radial and toroidal direction);
- manifolds region: 9^{th} degree polynomial function of one variable (radial direction);
- SPh regions: six different 8^{th}-10^{th} degree polynomial functions of two variables (radial and toroidal direction), one per region;
- SPv regions: five different 12^{th} degree polynomial functions of one variable (radial direction), one per region.

Hence, in the "multi-region" approach, the 13 different polynomial functions of one or two variables

selected allow a particularly accurate representation of the calculated thermal field, as it can be seen qualitatively in Figure 5.

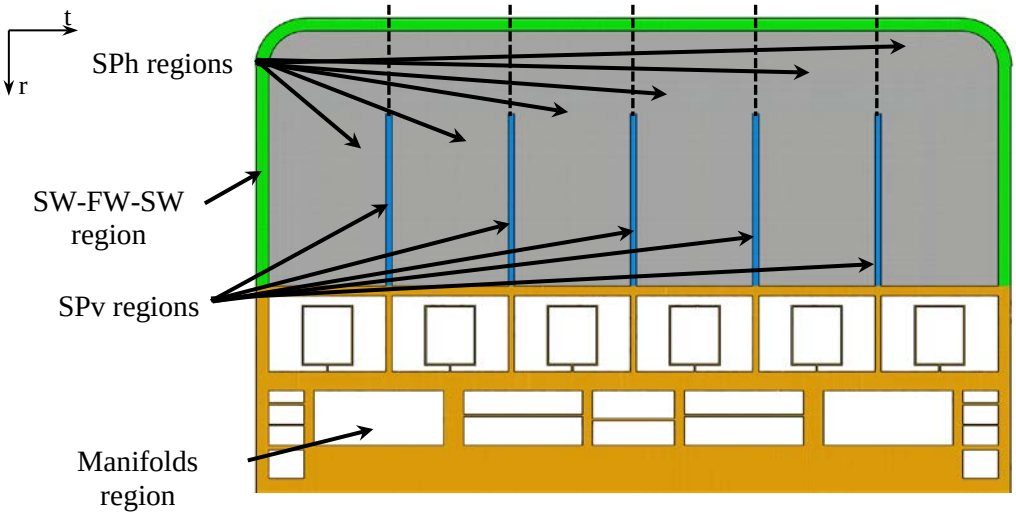

Figure 4. Interpolation strategies.

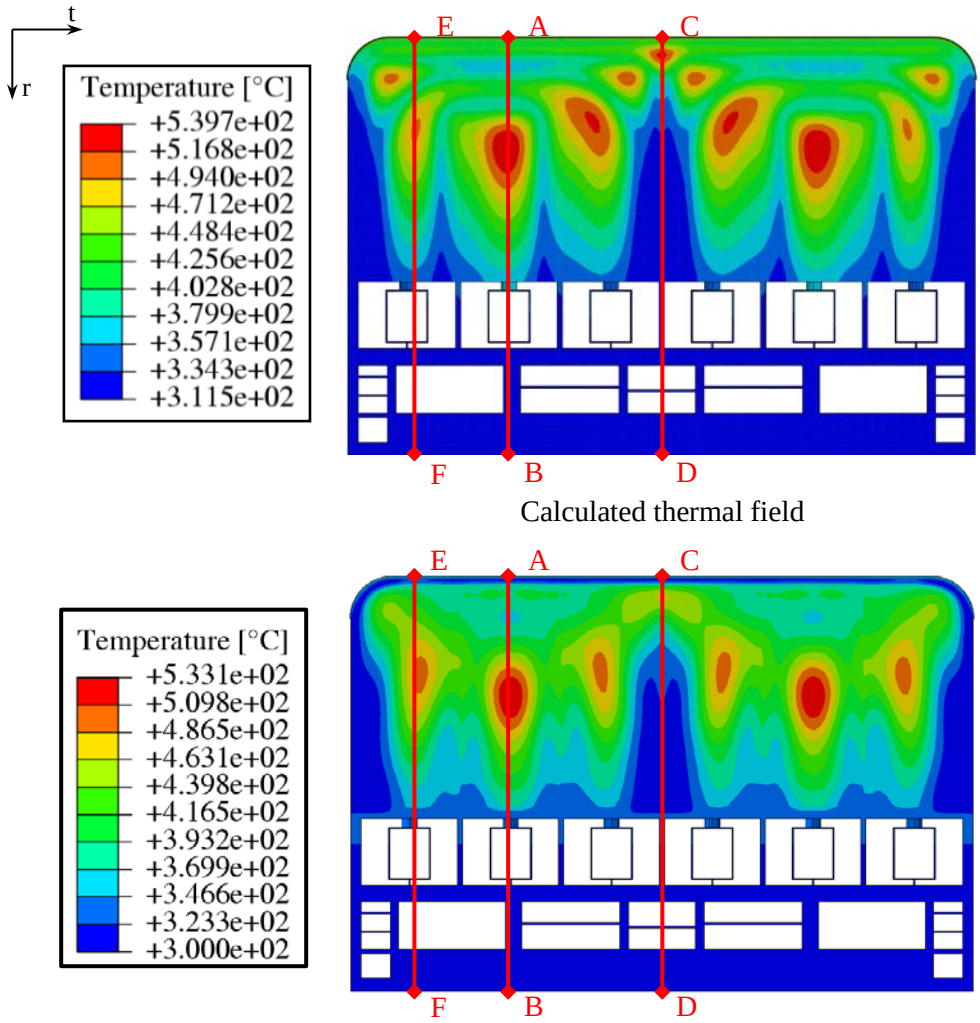

Figure 5. Calculated and interpolated thermal fields.

Moreover, in order to have a semi-quantitative comparison between the two thermal fields (namely calculated and interpolated), the temperature radial distributions obtained by the “multi-region” interpolation strategy has been compared to the calculated one, along the paths AB, CD and EF reported in Figure 5. The outcomes of this comparison, reported in Figure 6, allow confirming that the “multi-region” interpolation strategy shows a very good agreement with the calculated values.

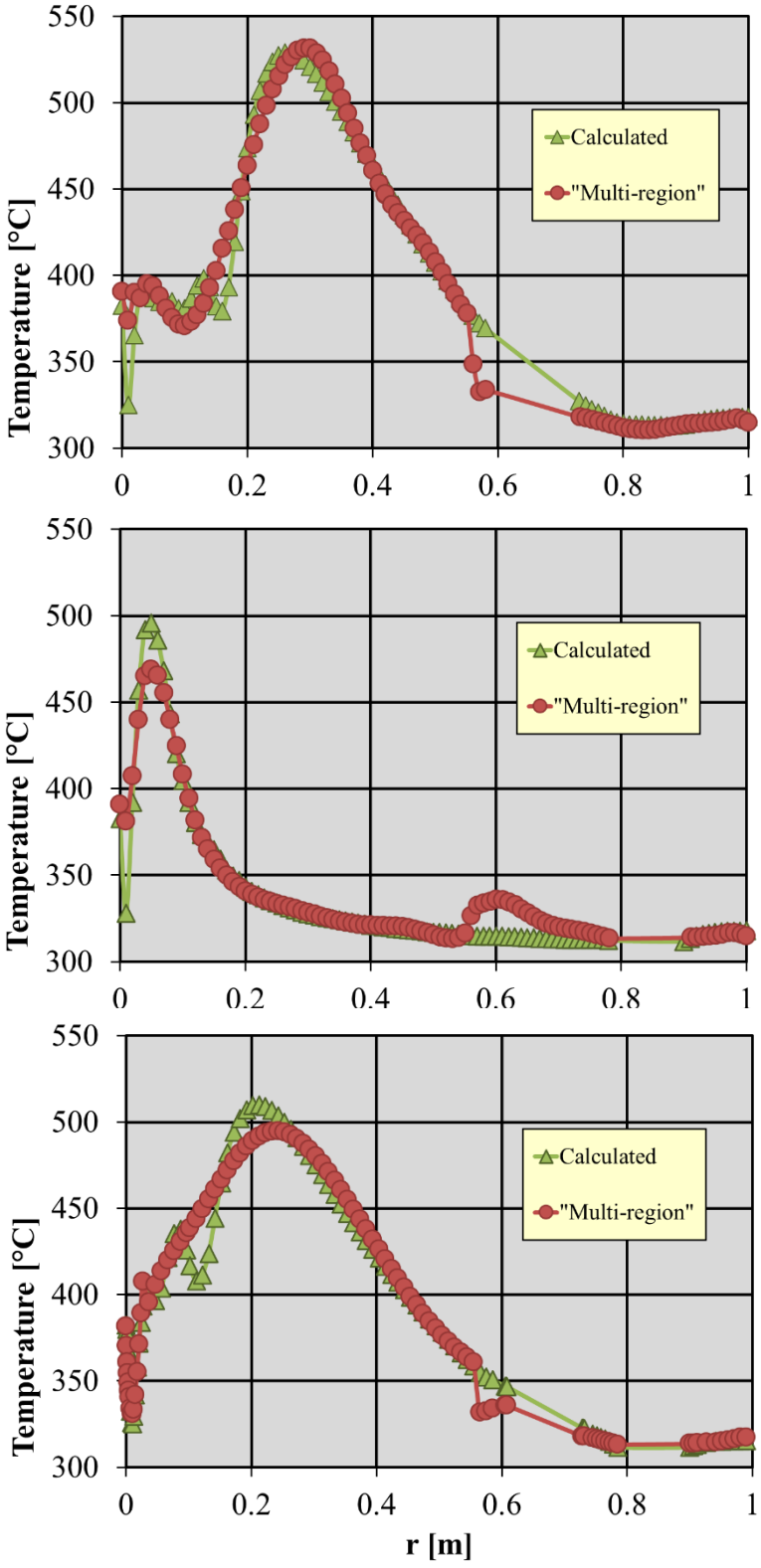

Figure 6. Radial temperature distributions along the considered paths.

In the end, a quantitative comparison between the calculated thermal field and that interpolated by the “multi-region” strategy has been performed. To this purpose, the contour map of the relative error, defined as the difference between the calculated temperature and the interpolated one divided by the calculated value, is shown in Figure 7. Moreover, the relative error statistical distribution is depicted in Figure 8 together with the associated cumulative curve.

As it can be observed, the highest relative error is predicted in the manifold region, where the temperature values are the lowest, and in between the BZ cooling tubes, where the three-dimensional distribution is more pronounced. In any case, as the latter regions are very localised, this loss of detail can be considered acceptable.

Moreover, the statistical distribution of the calculated relative error show that the most of the error values stays within the range ± 4%, with a peak around 0. Indeed, looking at the cumulative curve, about the 90 % of the relative error values stay within this range.

These outcomes allow concluding that the “multi-region” interpolation strategy is capable of matching the calculated thermal field with a very good agreement with the calculated data.

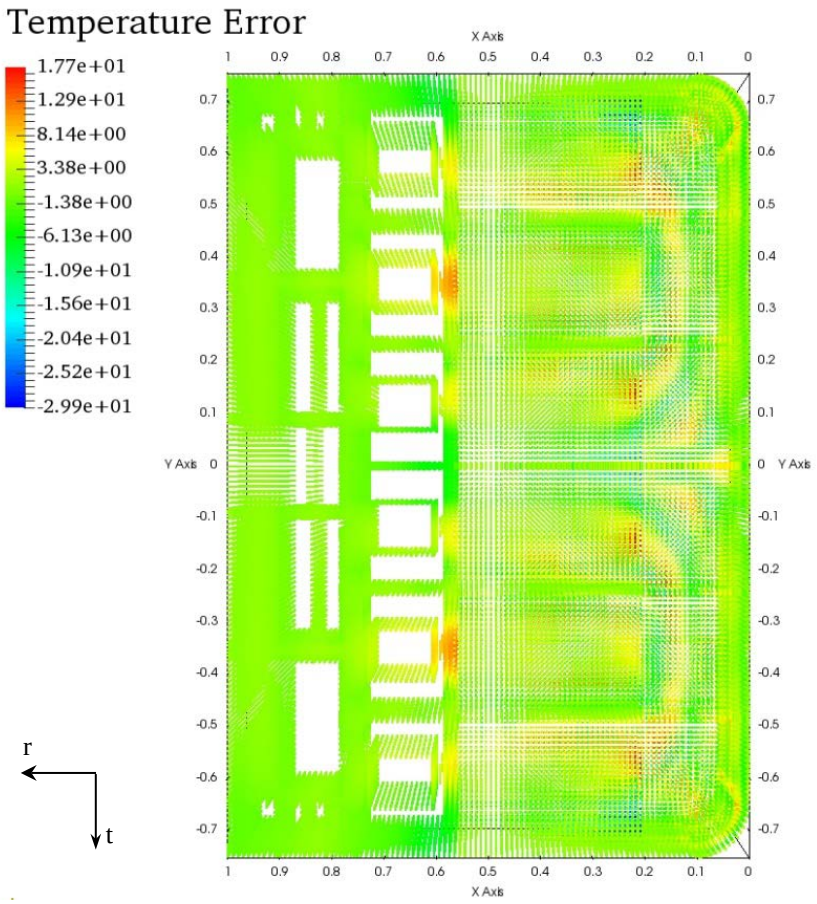

Figure 7. Contour map of the temperature error [in %] between the calculated thermal field and the “multi-region” interpolation.

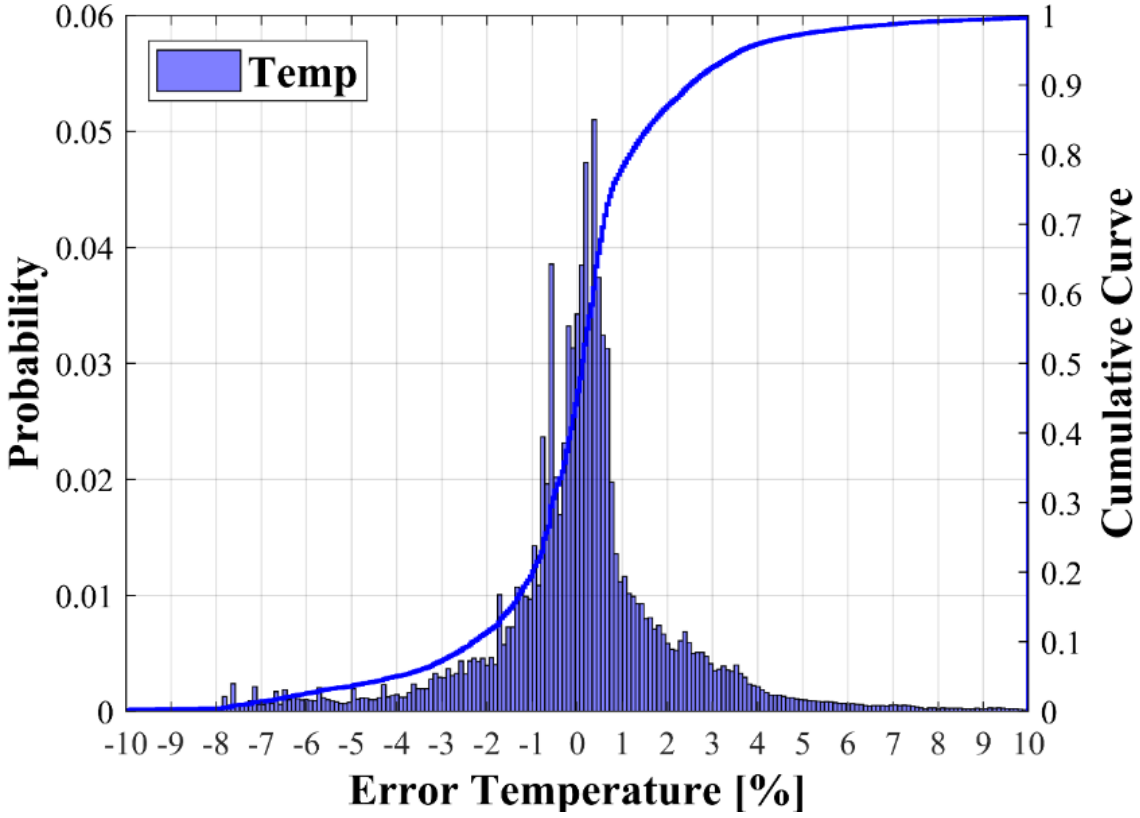

Figure 8. Statistical distribution of the error on temperature [in %] between the calculated thermal field and the "Multi-region" interpolation (histograms) and cumulative curve.

4. Structural analysis and comparison of the secondary stress fields

Once assessed the capability of the "multi-region" interpolation strategy of matching the calculated temperature field on a given spatial discretization grid, a quantitative comparison between the secondary stress fields originated by the calculated and the interpolated thermal fields has been performed.

To this purpose, a FEM model has been set-up on the same mesh already adopted for the thermal analysis. In particular, the set of mechanical boundary conditions shown in Figure 9 has been imposed in order to simulate the poloidal continuity of the assessed region as well as to reproduce the action of the WCLL BB attachment system devoted to mechanically connect the BB to the Vacuum Vessel. To this end, displacement of nodes lying onto the red and blue lines of Figure 9 has been prevented along radial and toroidal directions, respectively. Moreover, a symmetry condition along the vertical direction has been imposed to the nodes lying onto the lower radial-toroidal face, whereas a plane strain condition along the same direction has been assumed for the nodes lying onto the upper radial-toroidal face.

Since the scope of this comparison is to assess the secondary stress, no pressure load has been taken into account in the model. Hence, uniquely the thermal fields (calculated and interpolated) have been imposed as load for the steady state mechanical analysis.

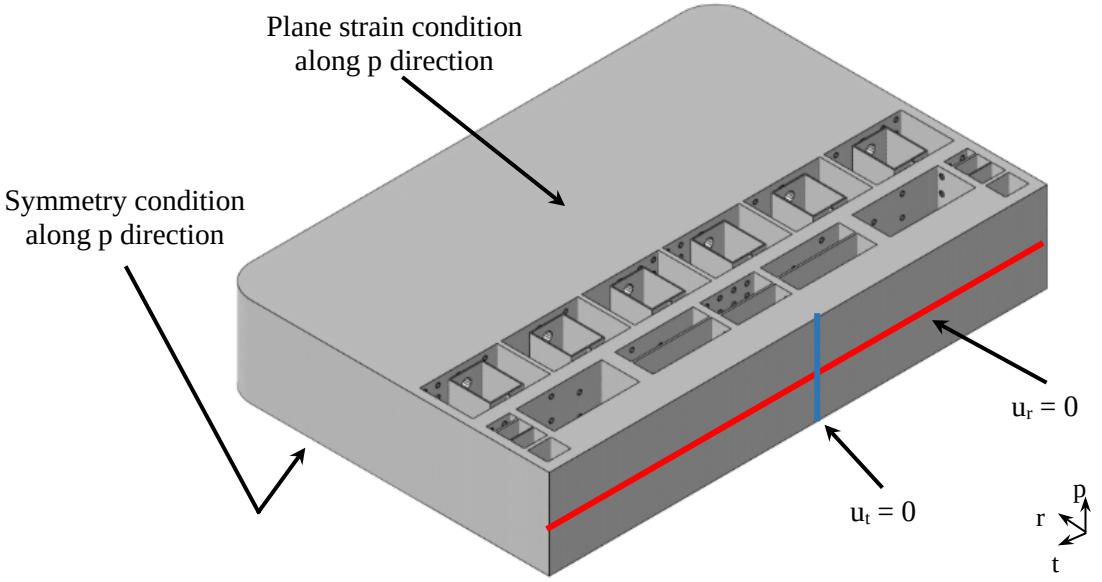

Figure 9. Boundary conditions.

Then, in order to compare the secondary stress arising within the central region of the WCLL COB segment as effect of the calculated and interpolated thermal fields, the spatial distributions of the stress tensor components S_{ij} have been considered. In particular, from Figure 10 to Figure 15, the S_{ij} spatial distributions predicted assuming the calculated thermal field are shown together with the spatial distribution of the relative error arising from the comparison between the S_{ij} values obtained from the calculated thermal field and those predicted assuming the interpolated temperature spatial distribution. The reported point to point comparison allow observing, as general remark, that the absolute value of the error is the highest (i. .e the error is greater than 50% or lower than -50 %, namely red and blue dots in figures from Figure 10 to Figure 15) where stress values are the lowest. Hence, it can be concluded that the interpolated thermal field allow predicting stress values with a good degree of reliability if compared with the analogous stress obtained from the calculated temperature spatial distribution. As a further demonstration, the statistical distributions of the error on stress prediction are reported in Figure 16. Here, it can be seen that error distributions present a peak near to 10-20 %, which can be considered acceptable error. Moreover, looking at the reported cumulative curves, it can be observed that, as to the normal stress components, about the 50 % of the relative error values stay within the range ± 20% whereas regarding the shear stress components about the 60 % of the relative error values stay within the same range. In addition, looking at the range ± 50%, one can see from the cumulative curves that it includes about the 80 % of the relative error values on the normal stress components and about the 90 % of the errors on the shear stress components.

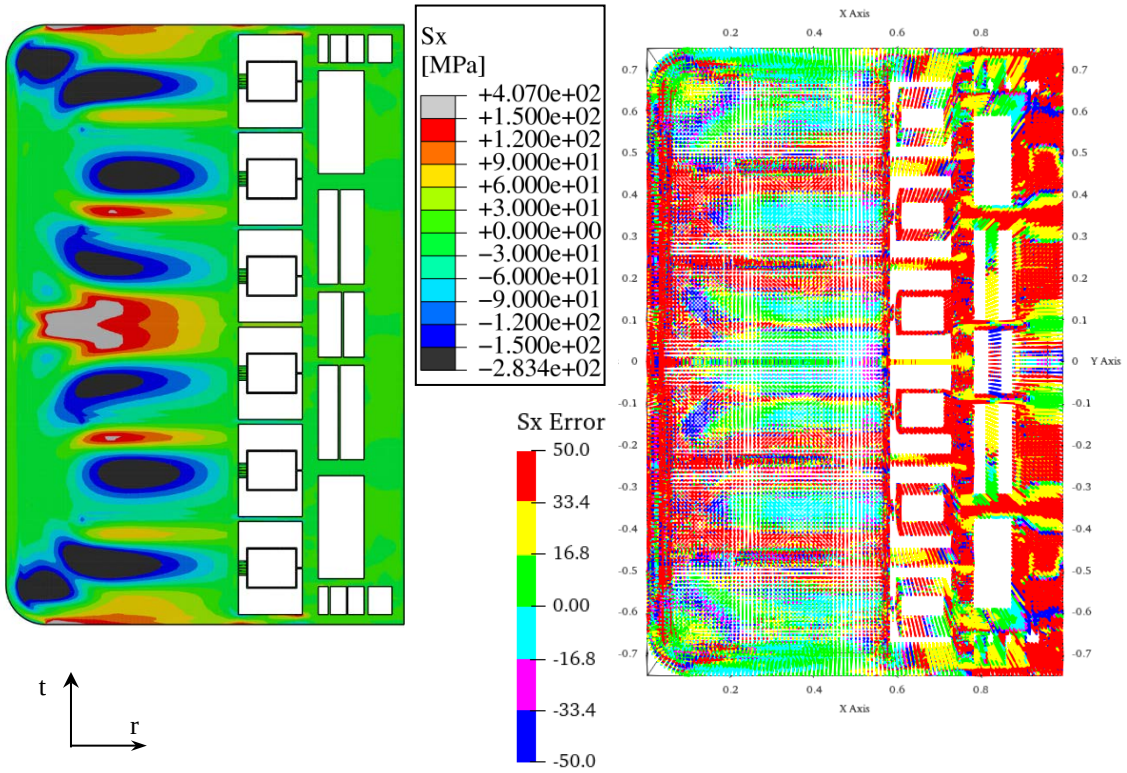

Figure 10. S_x spatial distribution from calculated thermal field (left) and relative error contour map (right) when compared with S_x from interpolated thermal field.

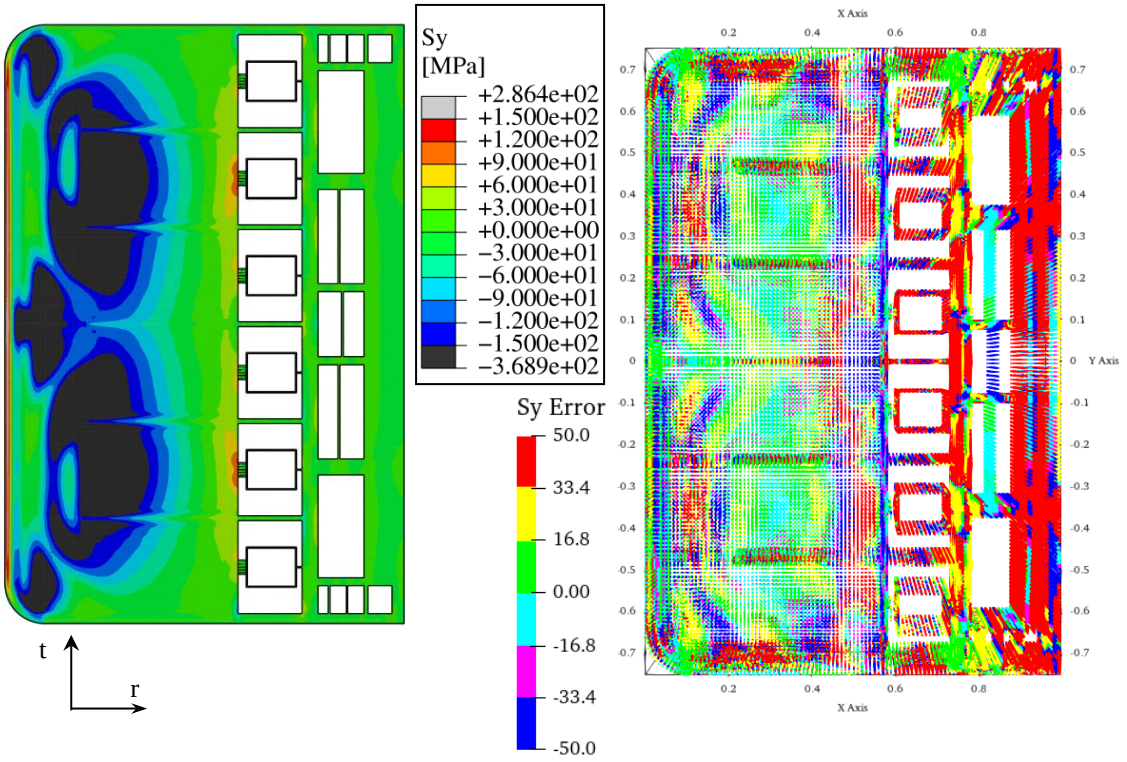

Figure 11. S_y spatial distribution from calculated thermal field (left) and relative error contour map (right) when compared with S_y from interpolated thermal field.

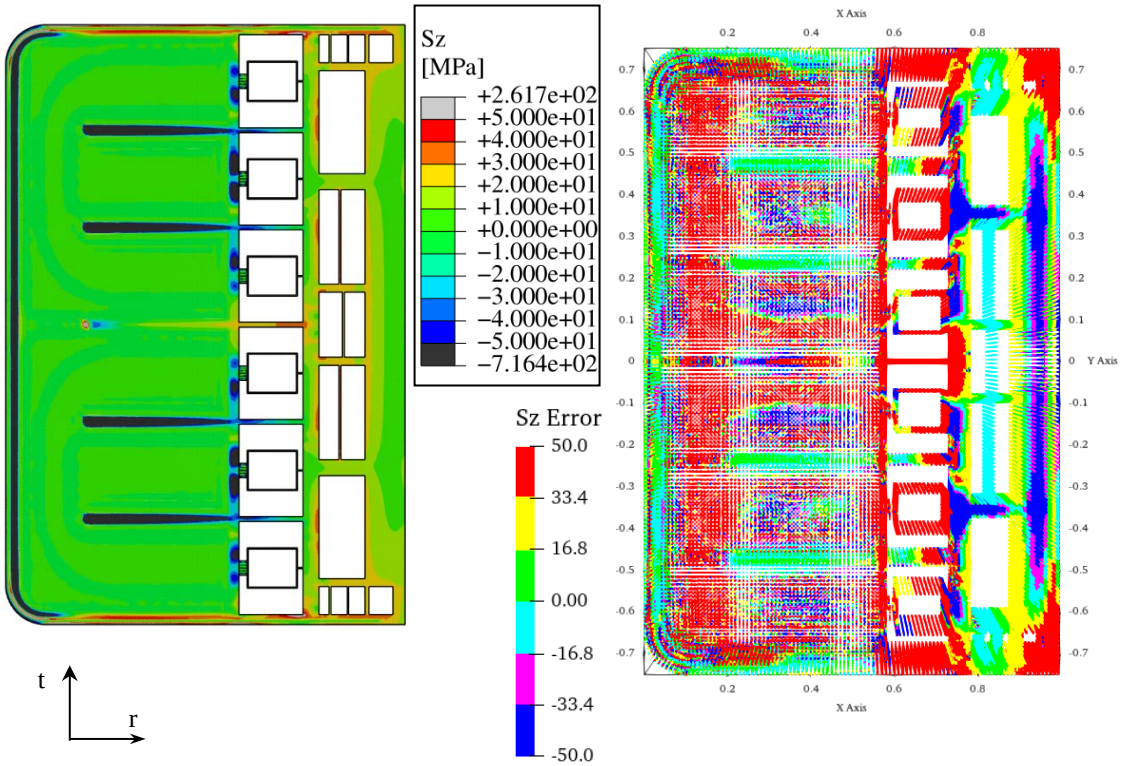

Figure 12. S_z spatial distribution from calculated thermal field (left) and relative error contour map (right) when compared with S_z from interpolated thermal field.

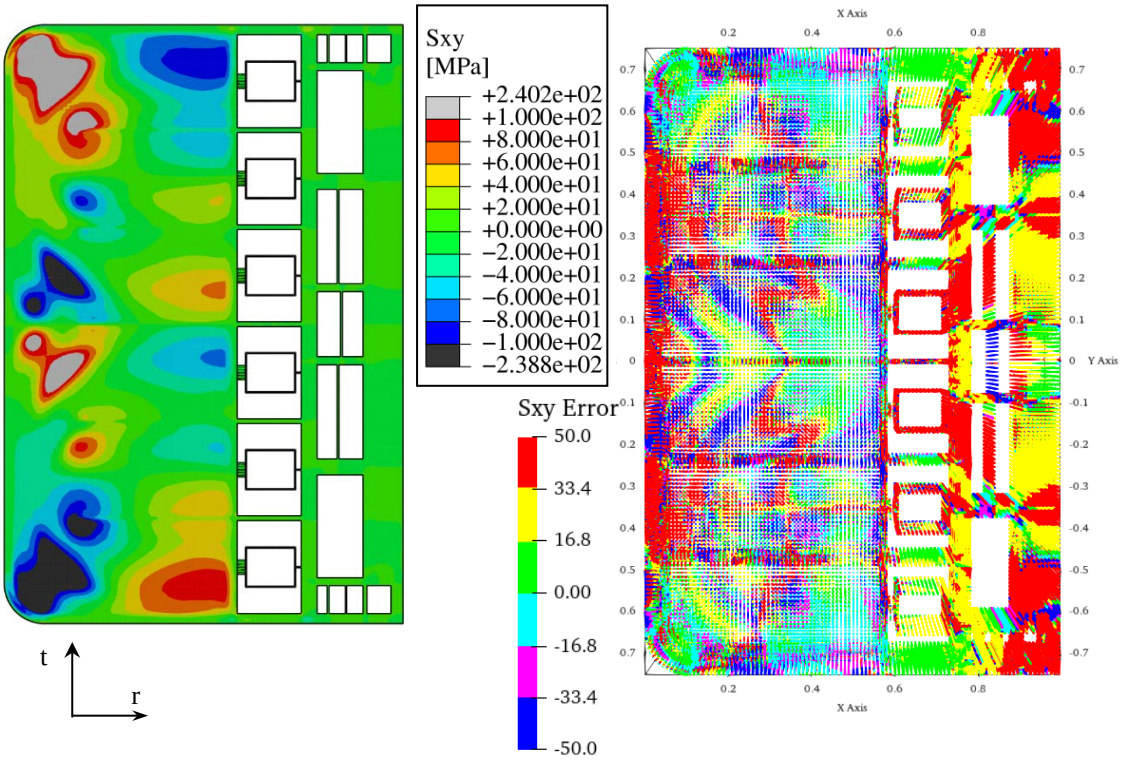

Figure 13. S_{xy} spatial distribution from calculated thermal field (left) and relative error contour map (right) when compared with S_{xy} from interpolated thermal field.

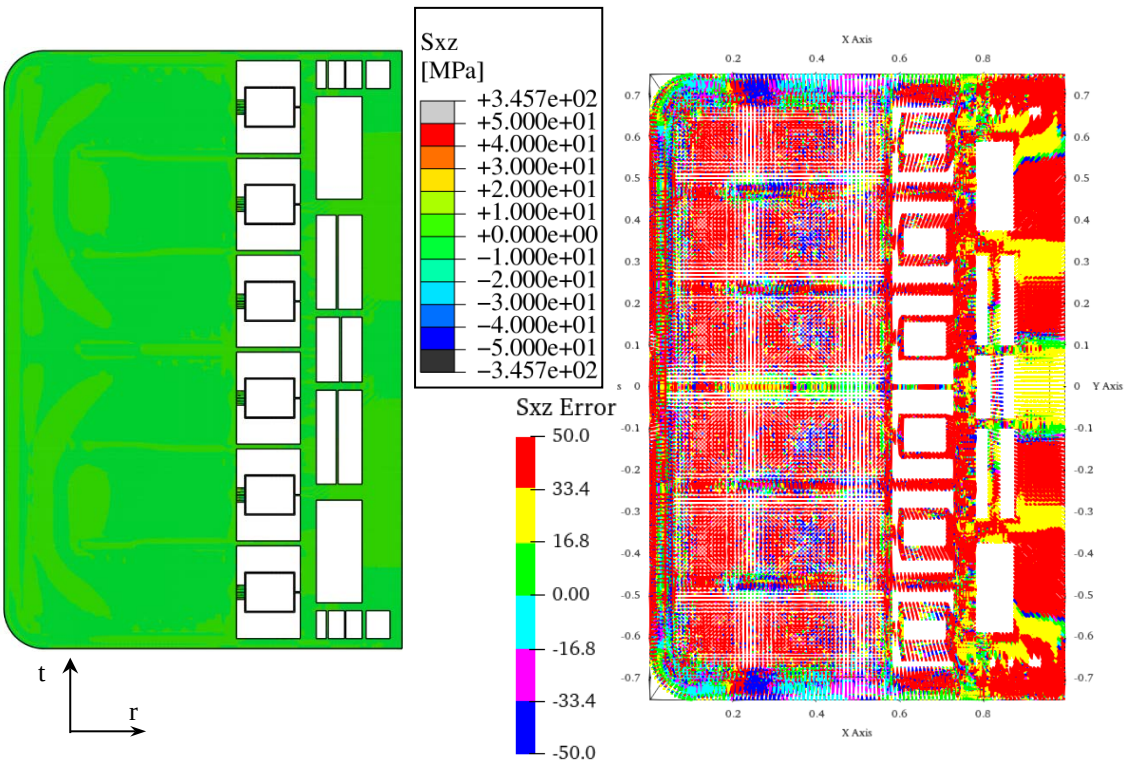

Figure 14. S_{xz} spatial distribution from calculated thermal field (left) and relative error contour map (right) when compared with S_{xz} from interpolated thermal field.

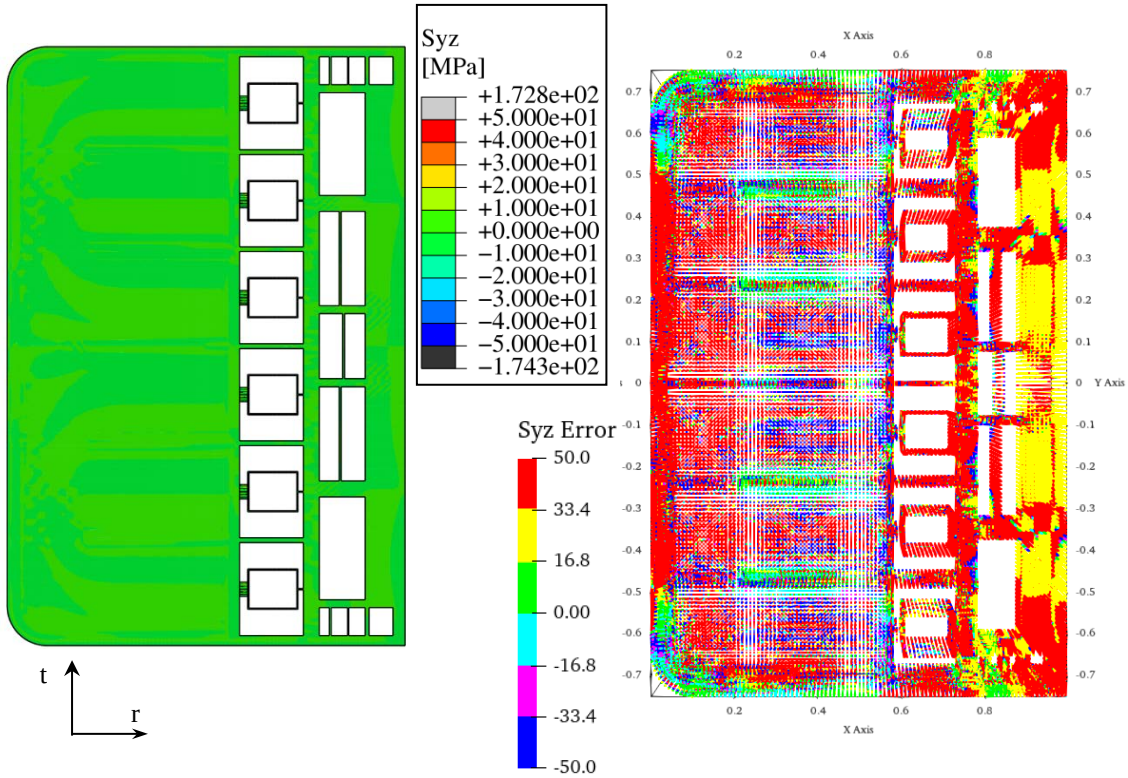

Figure 15. S_{yz} spatial distribution from calculated thermal field (left) and relative error contour map (right) when compared with S_{yz} from interpolated thermal field.

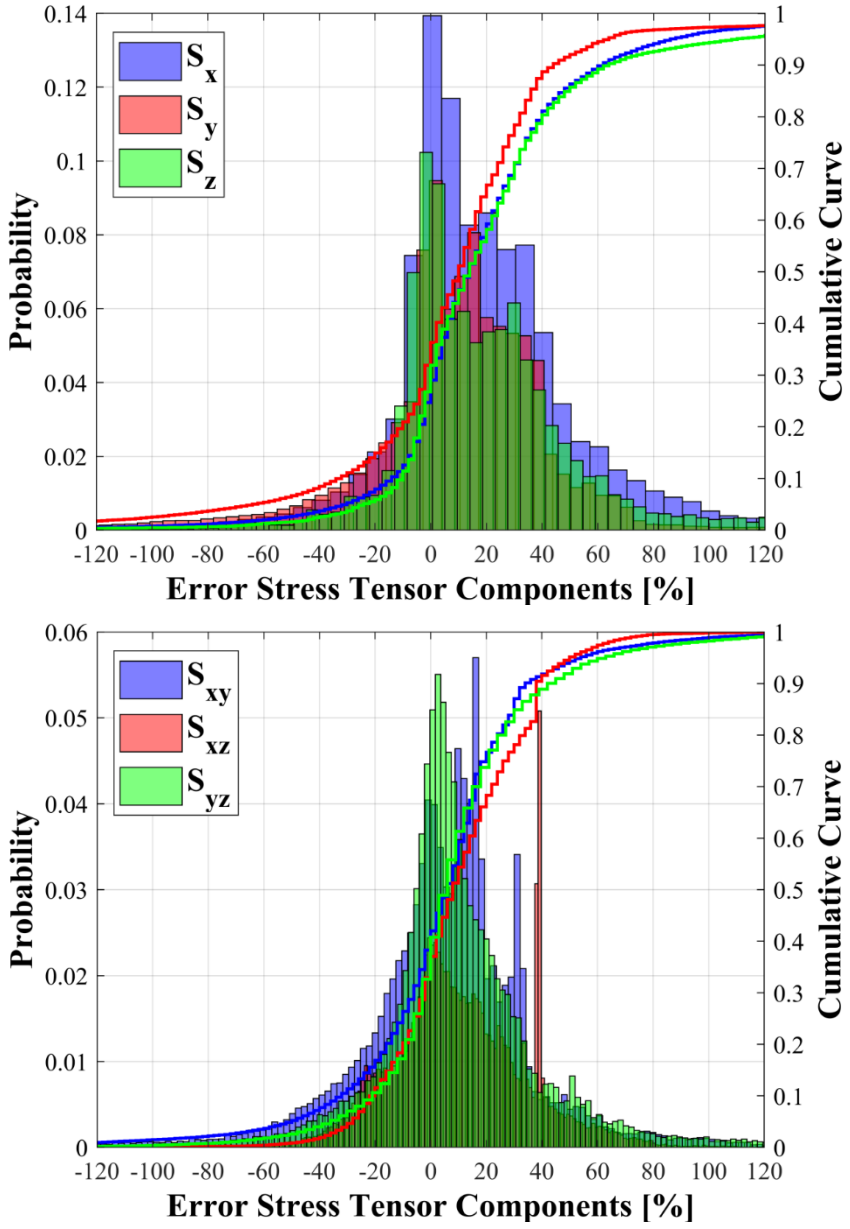

Figure 16. Statistical distribution of the error on S_{ij} between the calculated thermal field and the "Multi-region" interpolation (histograms) and cumulative curves.

5. Mesh independence assessment

Once proved the predictive power of the set of interpolating functions both in terms of temperature calculation and secondary stress prediction, a mesh independence assessment has been performed in order to verify that the promising outcomes obtained so fare are still valid for coarser meshes. Indeed, in sight of the application of the interpolated thermal field to a whole WCLL BB segment, a very coarse mesh is expected. To this purpose, five alternative meshes (Figure 17) have been set-up and their features are summarized in Table 1 together with the original mesh adopted so far.

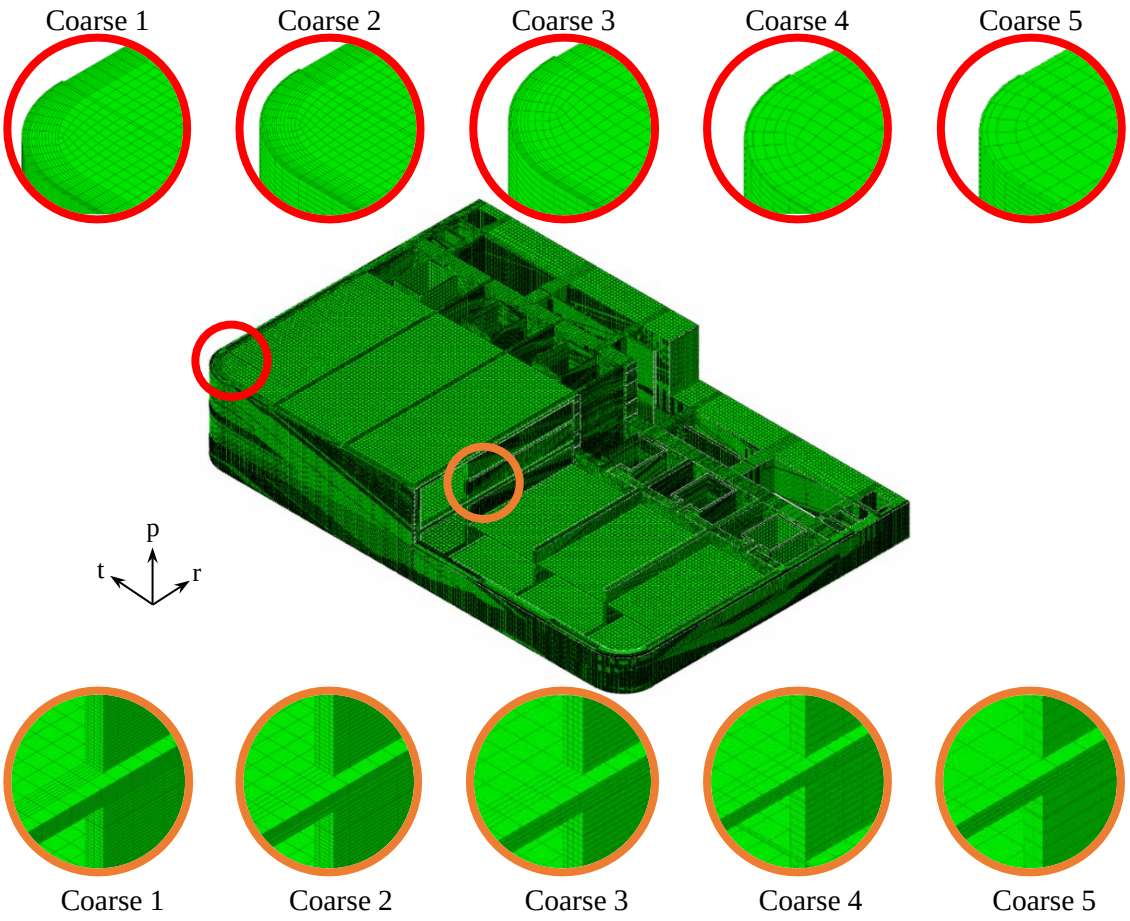

Figure 17. The coarse mesh set-up for the mesh independence study.

Table 1. Features of the coarser meshes set-up and comparison with the original one.

	Nodes	**Elements**	**Nodes % decrease**
Original mesh	1948580	1’627’736	/
Mesh 1	1’556’139	1’303’312	~20%
Mesh 2	1’037’463	826’294	~45%
Mesh 3	715’984	561’616	~65%
Mesh 4	312’738	224’328	~85%
Mesh 5	211’753	142’108	~90%

As a first comparison, the set of 13 polynomial functions has been applied to each of the 5 coarser mesh in order to reproduce the thermal field on them. After that, a proper thermal and thermo-mechanical analysis has been performed for each of the 5 coarse mesh. Then, each calculated thermal field has been compared with the “multi-region” interpolation field obtained on the same mesh and, in addition, each calculated secondary stress field has been compared to the stress field originated by the interpolated temperature distribution on the same mesh. About the thermal comparison, for the sake of brevity results concerning coarse meshes 1 and 5 are reported in Figure 18. As it can be seen, the statistical distribution of the percentage error is peaked on 0 %, with the most of the error ranging from -5% to 5% as indicated from the cumulative curves (in particular, about the 95-90 % of the error values

stay within this range for Coarse Mesh 1 and 5, respectively). In addition, it can be observed from the error contour maps that the highest errors are concentrated in the manifold regions, where the temperatures are low, and in between the DWTs, in very localized spots, where the 3D behaviour is more pronounced. Hence, this is a further proof of the high predictive power, in terms of temperature spatial distribution, of the “multi-region” interpolation procedure set-up.

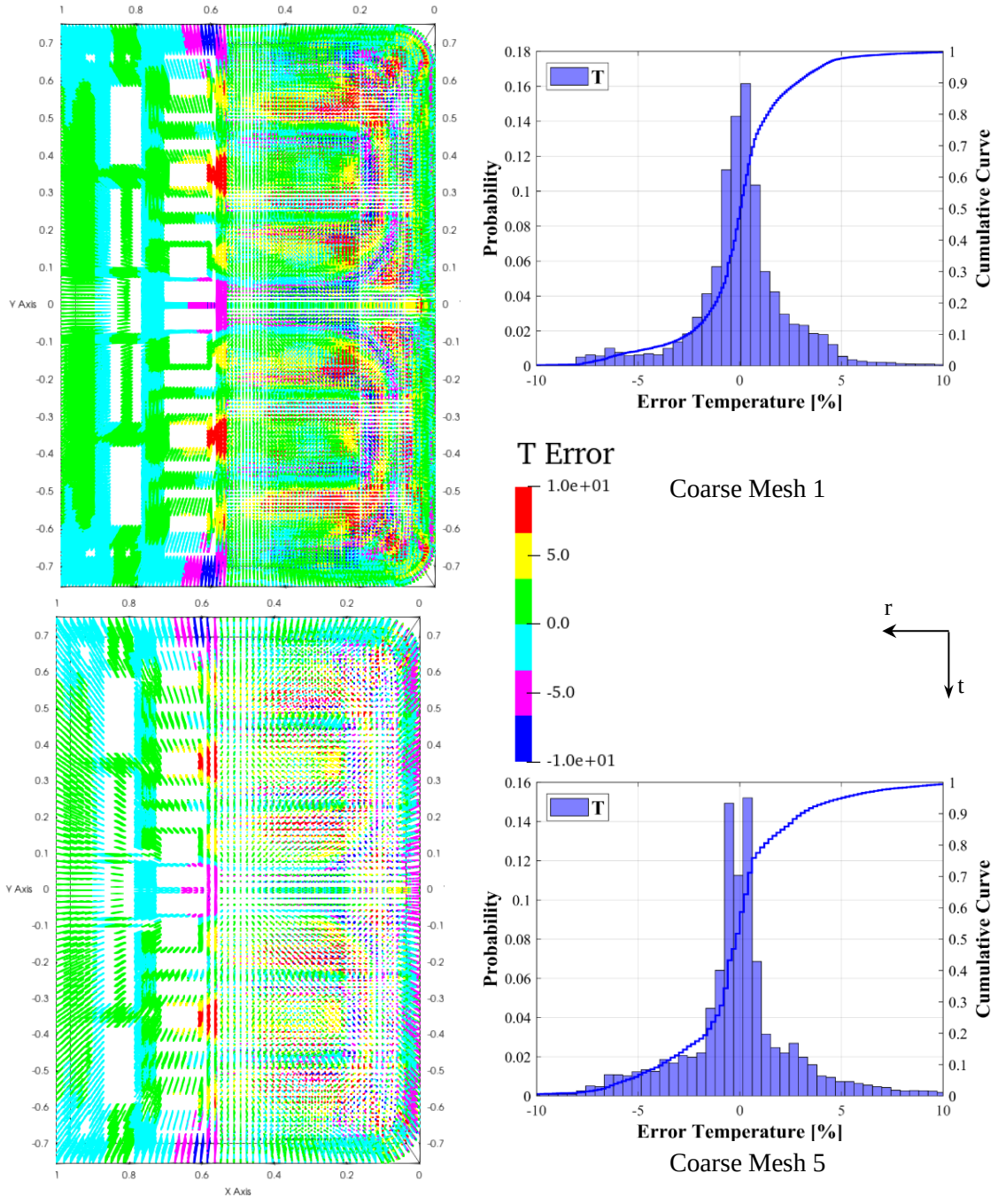

Figure 18. Error on temperature prediction for the coarser meshes 1 and 5.

Regarding the comparison between the secondary stress fields, results qualitatively similar to those already shown in figures from Figure 10 to Figure 15 are obtained for each of the 5 coarser meshes. As an example, results concerning the coarse Mesh 5 are reported from Figure 19 to Figure 25. Also in this case, the highest percentage error resulting from the comparison between the calculated thermal stress and that coming from the interpolated temperature arise where the stress are the lowest. In addition,

looking at the error statistical distributions and the associated cumulative curves, it can be seen that the most of the error values (~ 80 %) stay within the range ± 50 % with peaks in between ± 20 %. Hence, in principle, this allow concluding that the proposed procedure is viable for coarser meshes.

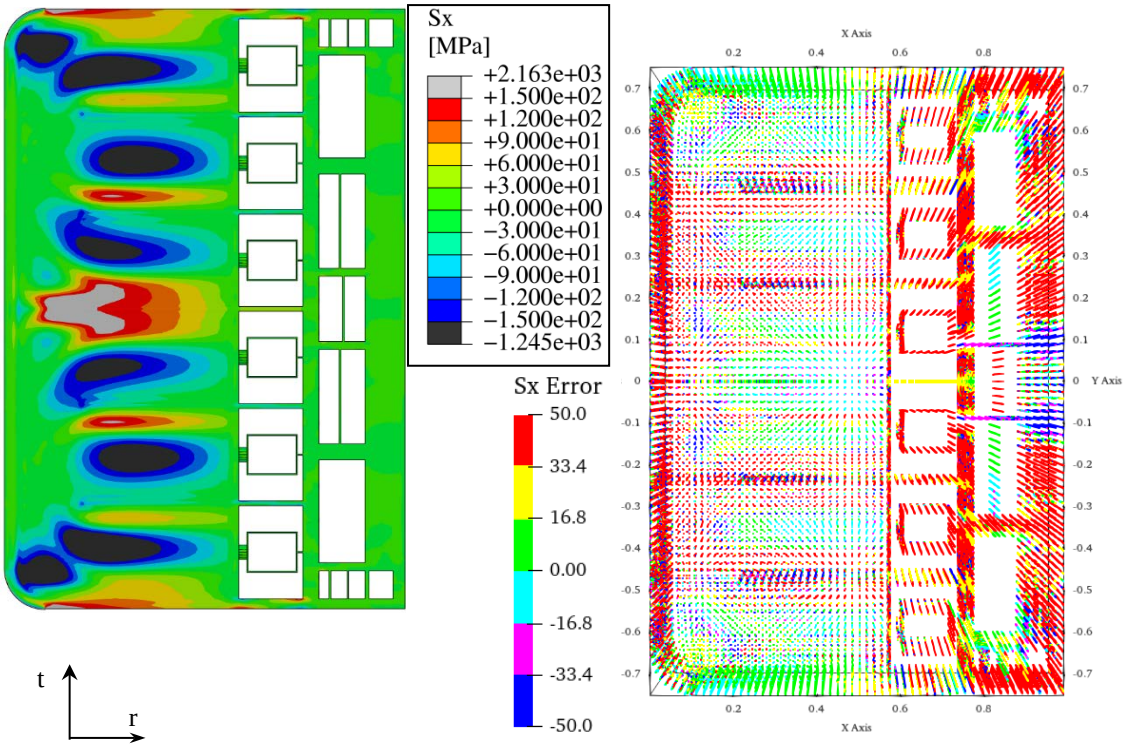

Figure 19. S_x spatial distribution from calculated thermal field (left) and relative error contour map (right) when compared with S_x from interpolated thermal field.

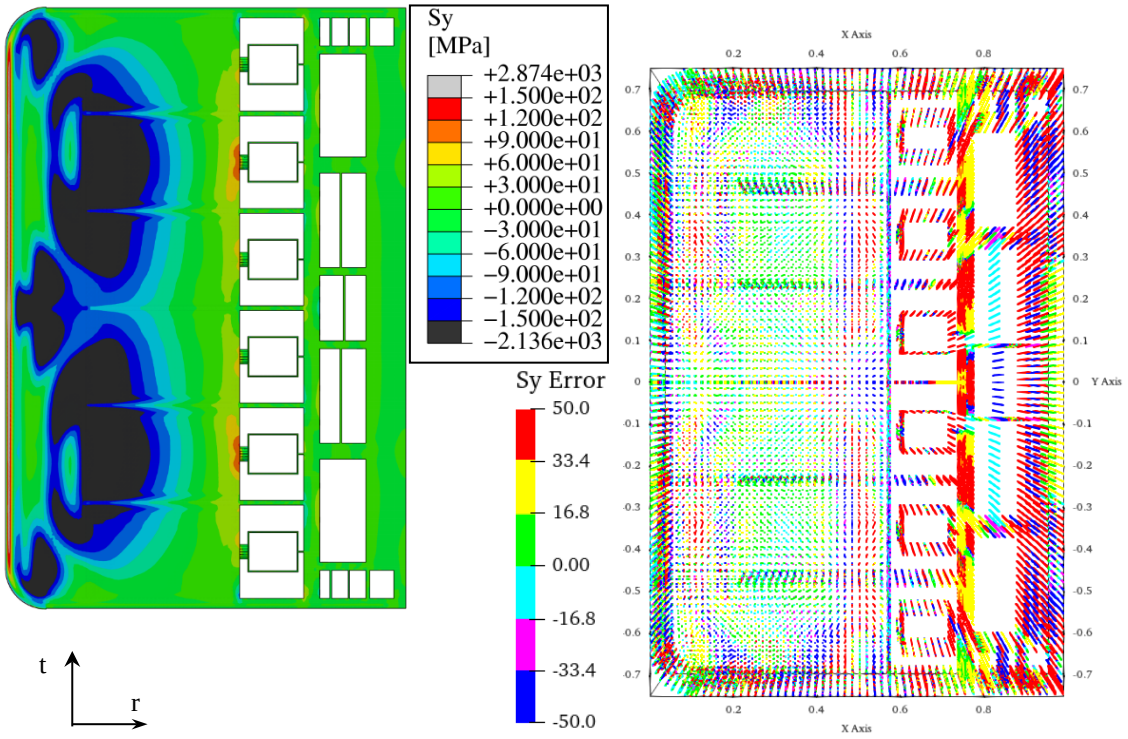

Figure 20. S_y spatial distribution from calculated thermal field (left) and relative error contour map (right) when compared with S_y from interpolated thermal field.

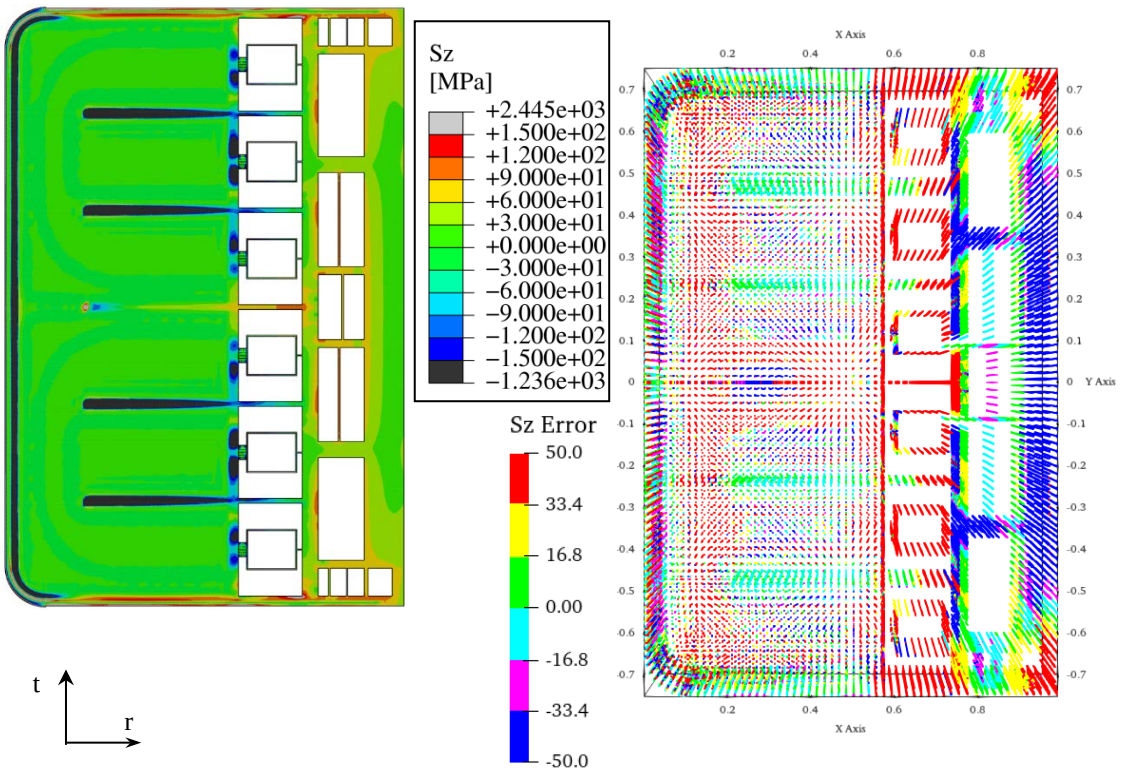

Figure 21. S_z spatial distribution from calculated thermal field (left) and relative error contour map (right) when compared with S_z from interpolated thermal field.

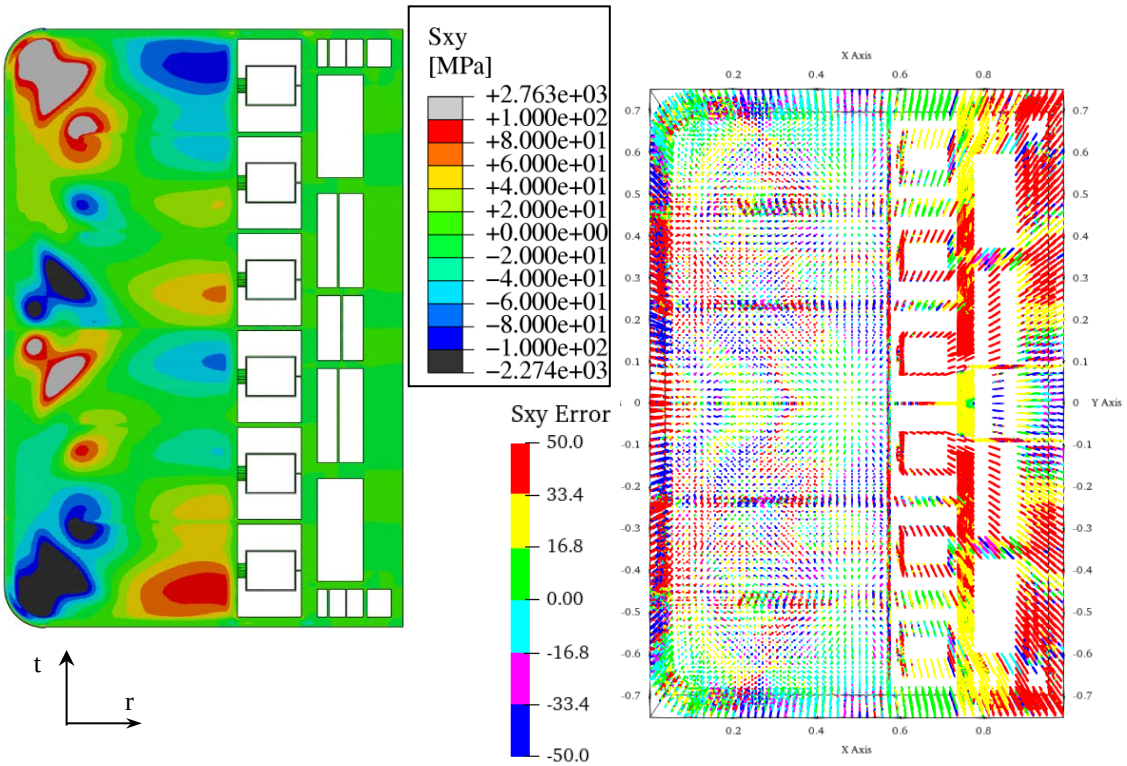

Figure 22. S_{xy} spatial distribution from calculated thermal field (left) and relative error contour map (right) when compared with S_{xy} from interpolated thermal field.

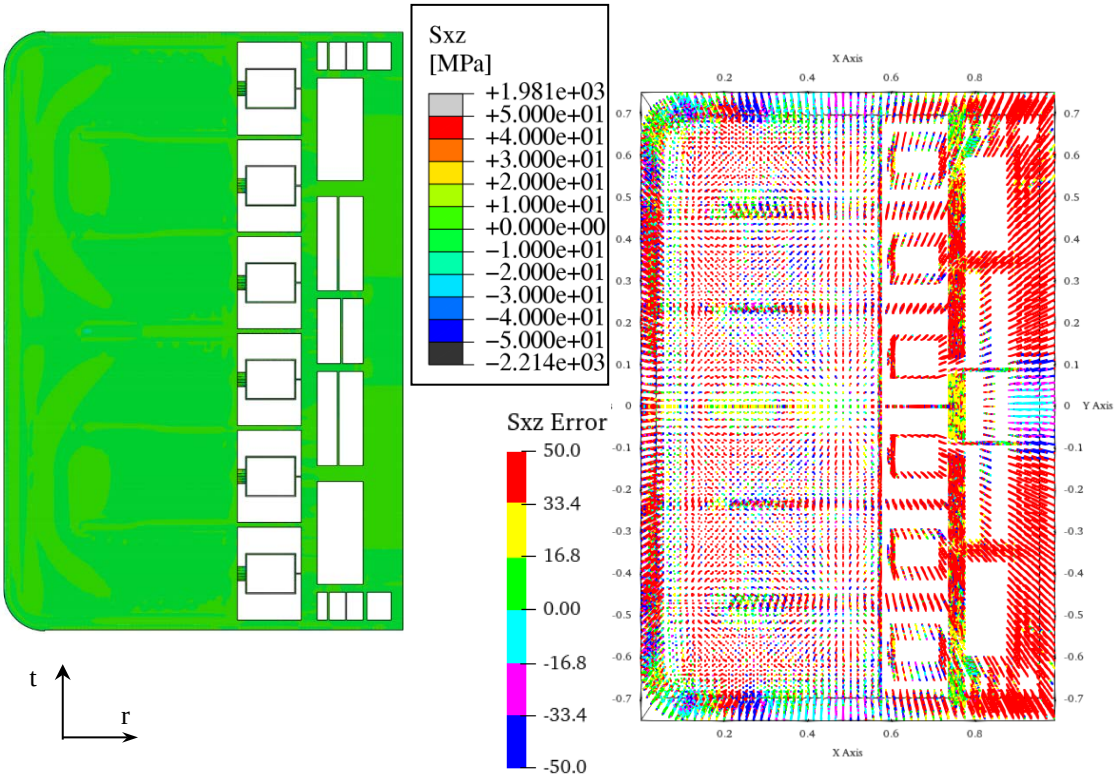

Figure 23. S_{xz} spatial distribution from calculated thermal field (left) and relative error contour map (right) when compared with S_{xz} from interpolated thermal field.

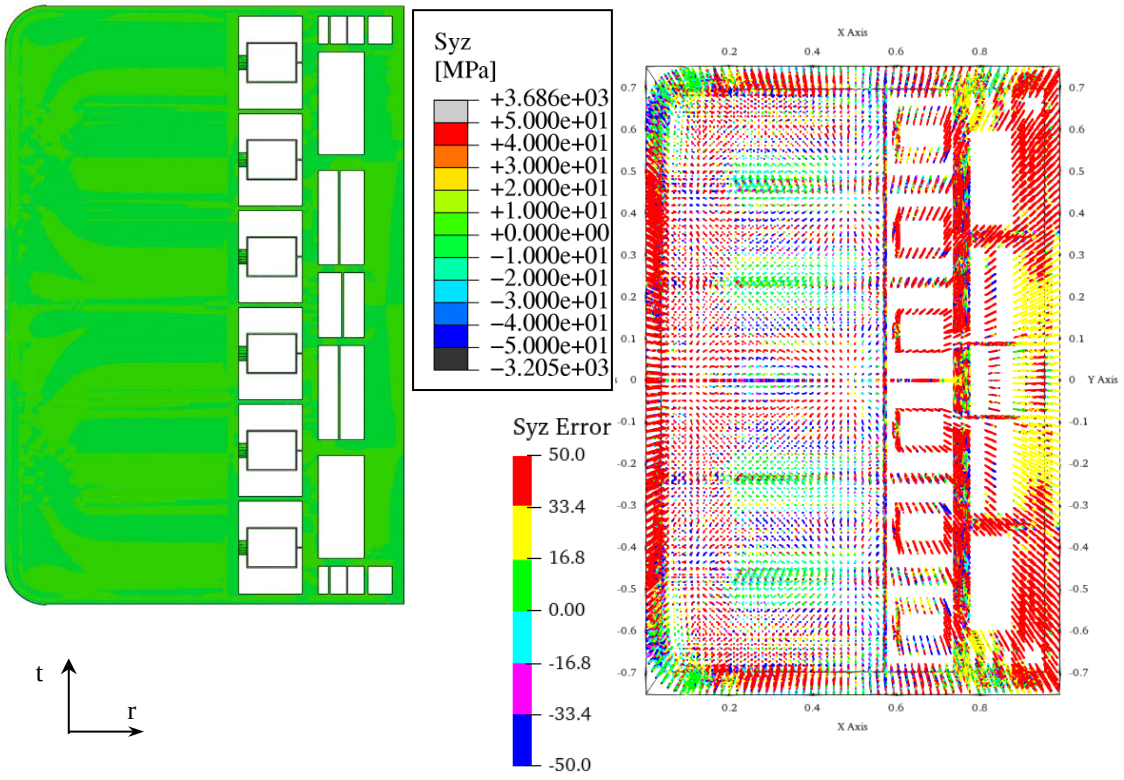

Figure 24. S_{yz} spatial distribution from calculated thermal field (left) and relative error contour map (right) when compared with S_{yz} from interpolated thermal field.

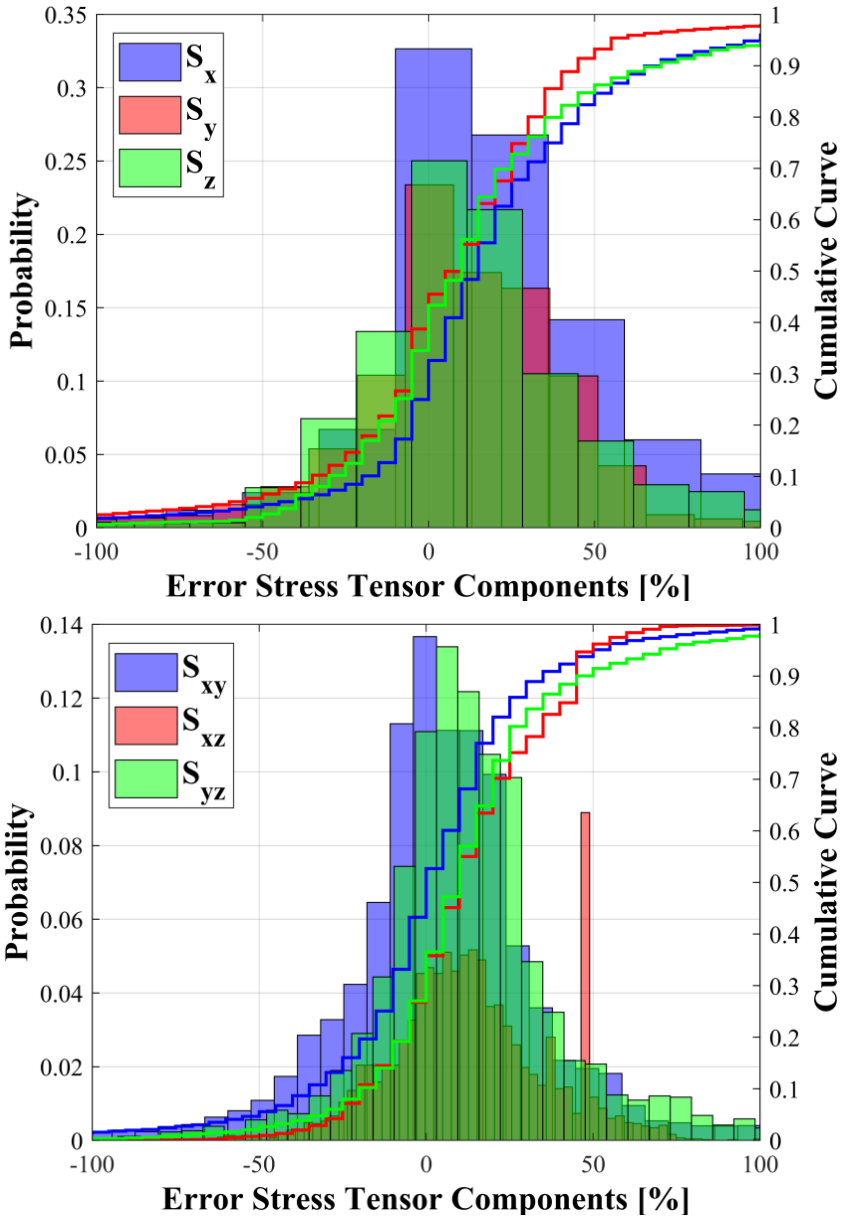

Figure 25. Statistical distribution of the error on S_{ij} between the calculated thermal field and the "Multi-region" interpolation (histograms) and cumulative curves.

6. Thermo-mechanical analysis of the WCLL COB segment

Once assessed the predictive power of the "multi region" interpolation strategy, either in terms of temperature and stress values prediction, the set of polynomial functions has been used for the thermo-mechanical analysis of the whole WCLL COB segment. The geometric layout of the considered segment is depicted in Figure 26, where the attachment system devoted to connecting the BB segment to the vacuum vessel is shown too. The reference attachment system configuration consists of a set of mechanical keys able to ensure the connection between BB and vacuum vessel, without using screws and/or bolts in order to simplify the remote maintenance operations.

In order to assess its thermo-mechanical performances, a mesh composed of ~2.3M nodes connected in ~4.6M tetrahedral and hexahedral linear elements has been set-up. Since the scope of this analysis was to predict the secondary stress field arising within the WCLL COB, the thermal field obtained using the "multi-region" interpolation field has been applied (Figure 27).

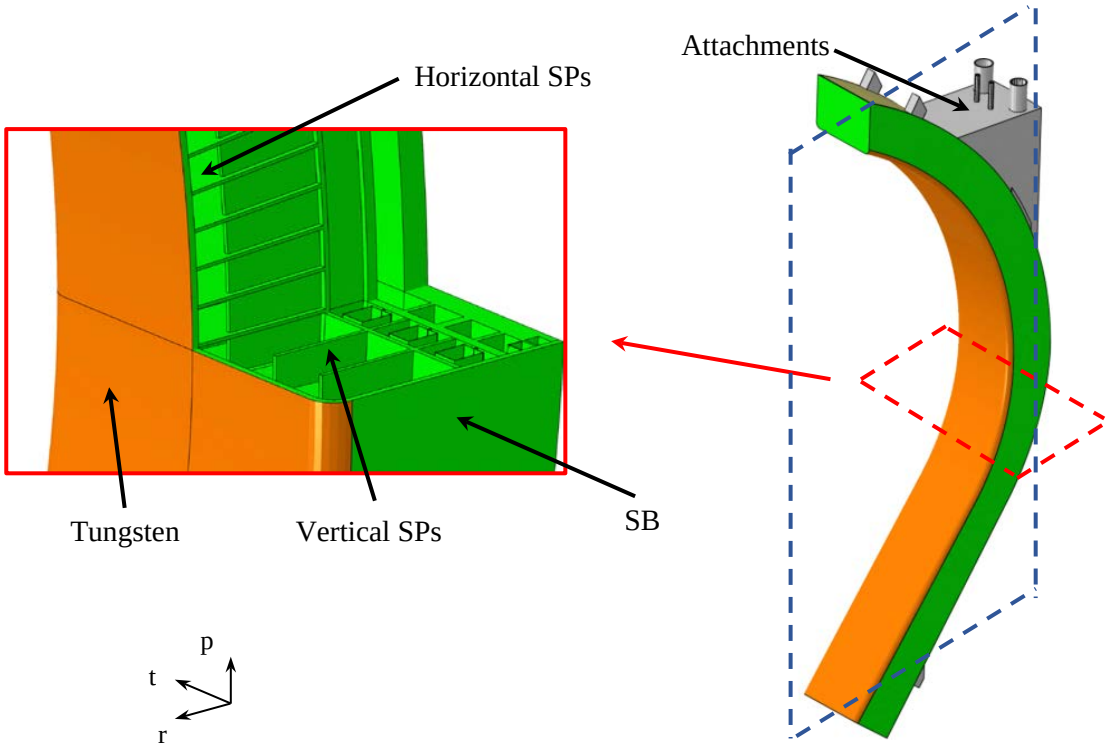

Figure 26. The WCLL COB segment

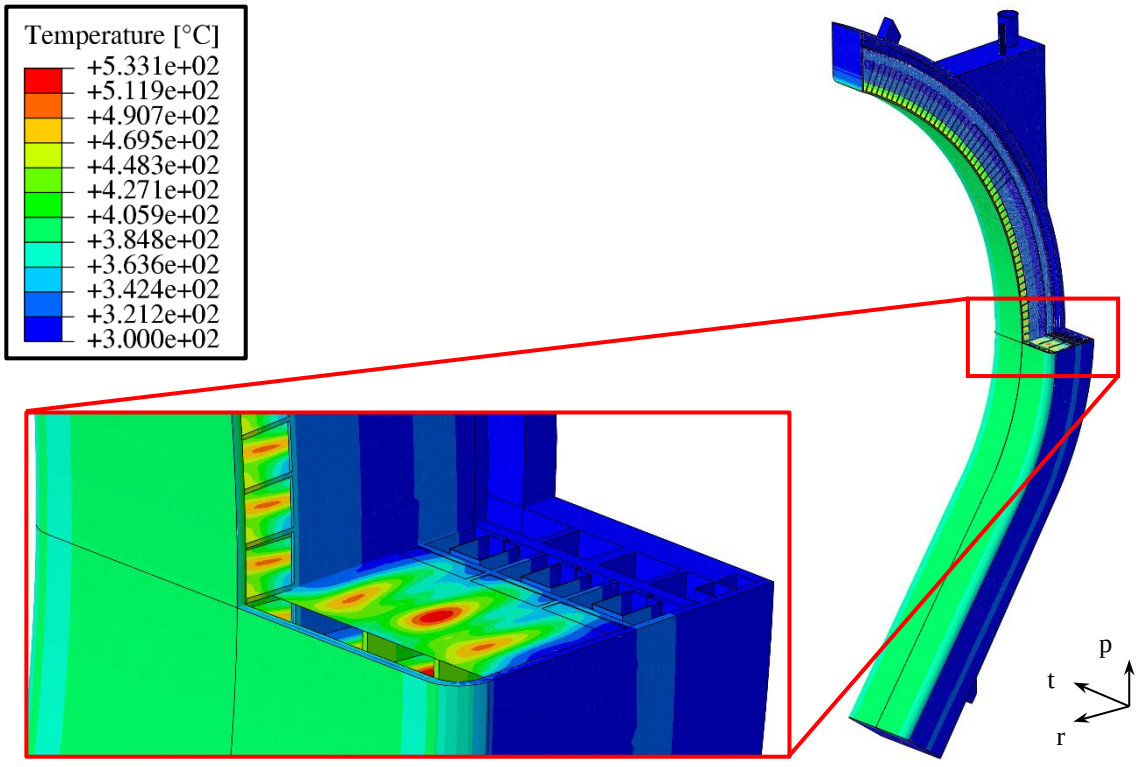

Figure 27. The “multi-region” interpolated thermal field applied to the whole WCLL COB segment.

As to mechanical restraints, in Figure 28 the regions highlighted in red represent the areas of the attachments in contact with the VV, each working along the direction indicated by the arrows in the figure. In particular, in the FEM model, their actions have been simulated by means of special spring elements with axis oriented along the specific working direction. Their elastic constants have been

calculated in order to correctly simulate the connection between BB and VV, as reported in [11].

Then, the secondary stress field has been calculated by means of a steady state structural analysis. The predicted Von Mises equivalent stress field is reported in Figure 29.

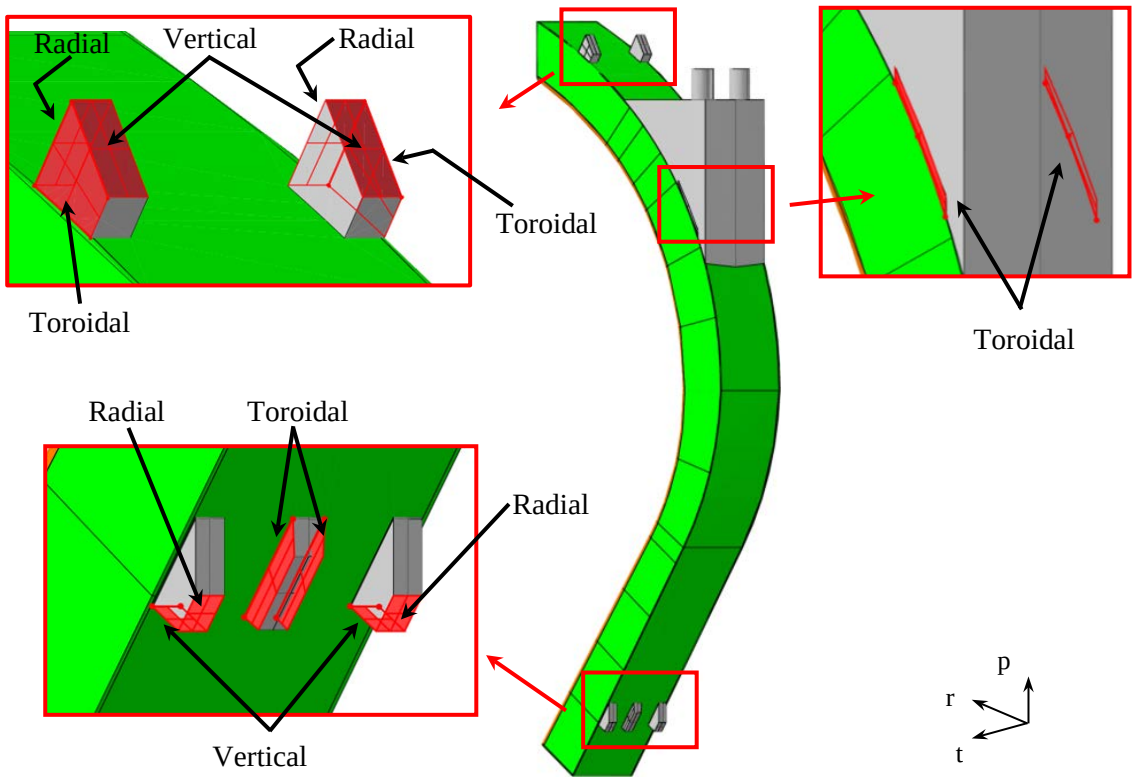

Figure 28. The attachment system

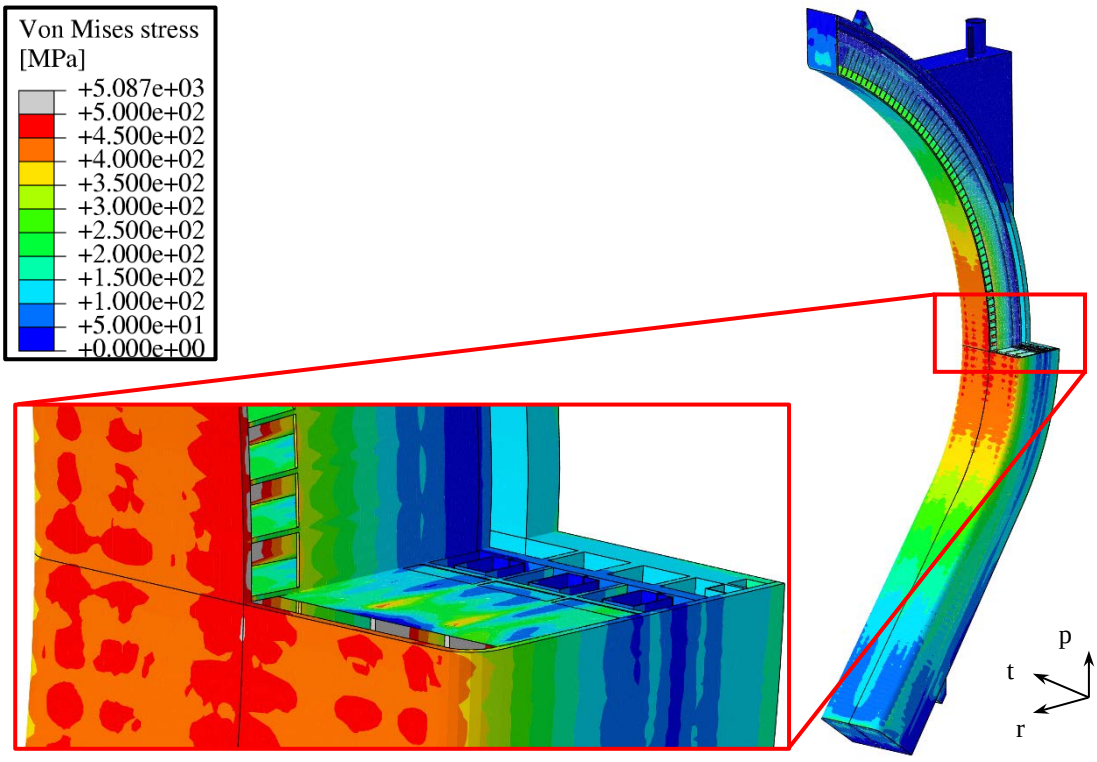

Figure 29. The Von Mises equivalent stress (secondary) calculated.

Adopting the procedure presented in this work, it is possible obtaining a remarkable level of detail in the stress field, otherwise not predictable. For instance, it is possible considering the effect of the SB cooling channels even though they are not modelled in the WCLL COB segment, since the assumed thermal field is derived from a local model endowed with the detailed FW channels layout. Moreover, as depicted in Figure 30, a remarkable difference in the stress spatial distribution within SPs can be observed comparing the obtained stress field (originated from the "multi-region" interpolation approach) with a different secondary stress field originated by a purely radial temperature profile given by a unique polynomial function. In particular, as shown in figure, an increased stress toroidal dependence can be obtained adopting the "multi-region" interpolation strategy for the thermal field.

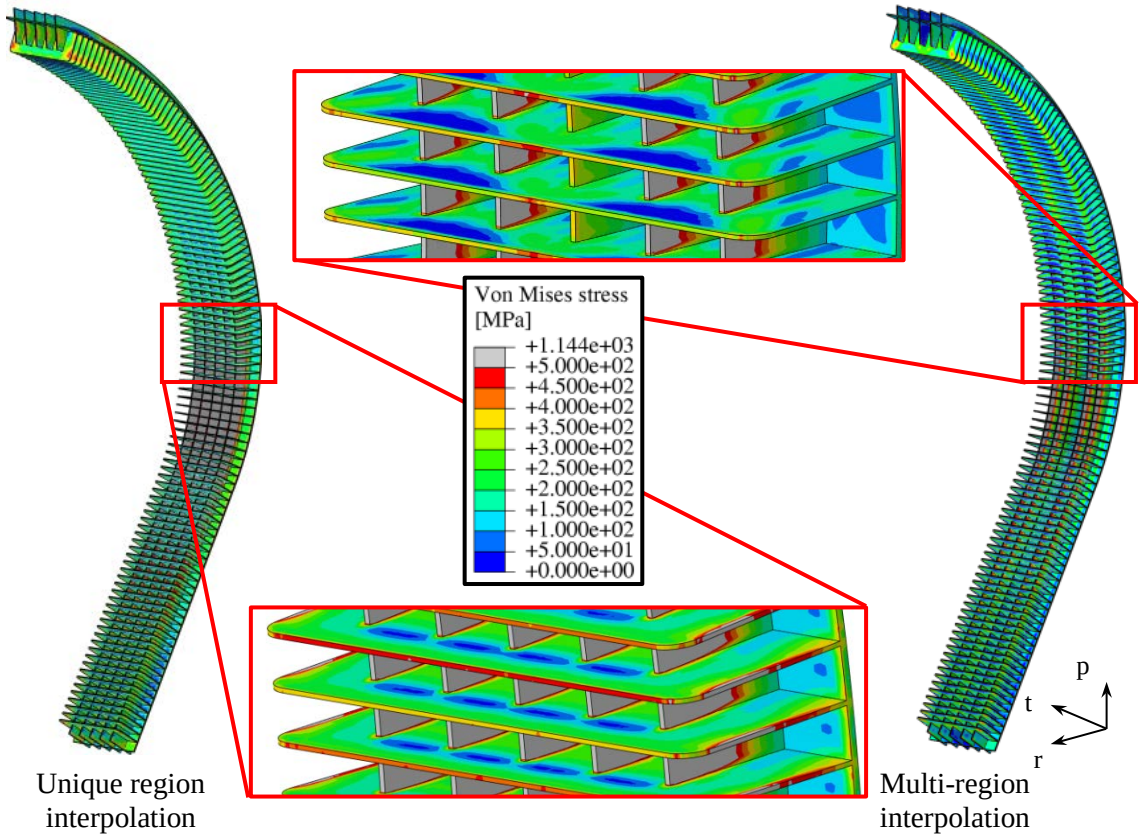

Figure 30. Comparison between secondary stress fields in the SPs geometric domain.

In any case, the adoption of the interpolation strategy, regardless of its level of detail, allows predicting results more reliably than in the past where the thermal field arising within the BB segments was assumed on the basis of rough considerations [12] or estimated averaging results of local analysis [13].

7. Conclusion

In the present work, a set of polynomial functions of the radial and toroidal variable has been found in order to interpolate the thermal field of the equatorial region of the WCLL COB segment, in sight of its application to the whole segment. Such a kind of interpolation procedure, called "multi-region" strategy, allows imposing a realistic thermal field to the whole segment without performing its full thermal-hydraulic assessment. The mesh independence of the "multi-region" interpolation strategy has been assessed and confirmed, both in terms of temperature and thermal-induced stress prediction, with

an acceptable error. This leads to the conclusion that the adopted strategy can be used to assess the thermo-mechanical behaviour of the whole BB segment with a good level of confidence. Hence, the calculation of the secondary stress on the whole WCLL COB segment, based on the thermal field imposed by means of the found set of interpolating functions, has been performed.

In principle, the adopted procedure can be applied to all the BB segments once known the temperature spatial distribution within a local region. Moreover, the interpolation procedure can be further improved, dividing the segment in a certain number of poloidal sub-segments (for instance upper, middle and lower sub segment), deriving for each sub-segment a proper set of interpolating functions from the thermal analysis of its central region and then applying to the whole segment a thermal field given by the stitching of the different sets of interpolating functions. This could allow an even more realistic prediction of the secondary stress arising within the WCLL COB segment.

Acknowledgments

This work has been carried out within the framework of the EUROfusion Consortium and has received funding from the Euratom research and training programme 2014-2018 and 2019-2020 under grant agreement No 633053. The views and opinions expressed herein do not necessarily reflect those of the European Commission.

References

[1] T. Donné et al., European Research Roadmap to the Realisation of Fusion Energy, EUROfusion, 2018 (ISBN 978-3-00-061152-0).

[2] F. Cismondi et al., Progress of the conceptual design of the European DEMO breeding blanket,tritium extraction and coolant purification systems, Fusion Engineering and Design, Vol. 157, 2020, pp. 111640, https://doi.org/10.1016/j.fusengdes.2020.111640.

[3] G. Federici et al., An overview of the EU breeding blanket design strategy as an integral part of the DEMO design effort, Fusion Engineering and Design, Vol. 141, 2019, pp. 30-42, https://doi.org/10.1016/j.fusengdes.2019.01.141.

[4] I. Catanzaro et al, Structural assessment of the EU-DEMO WCLL Central Outboard Blanket segment under normal and off-normal operating conditions, Fusion Engineering and Design, Vol. 167, 2021, pp. 112350, https://doi.org/10.1016/j.fusengdes.2021.112350.

[5] S. D'Amico et al., Preliminary thermal-hydraulic analysis of the EU-DEMO Helium-Cooled Pebble Bed fusion reactor by using the RELAP5-3D system code, Fusion Engineerind and Design, Vol. 162, 2021, pp. 112111, https://doi.org/10.1016/j.fusengdes.2020.112111.

[6] A. Del Nevo et al., WCLL BB design and Integration studies 2019 activities, Final Report on Deliverable, EUROfusion, EFDA_D_2P5NE5, http://idm.euro-fusion.org/?uid=2P5NE5, 2020.

[7] Material Property Handbook pilot project on Eurofer97 (MTA EK, KIT), IDM Ref. EFDA_D_2MRP77, 24/02/2016

[8] D. Martelli et al., Literature review of lead-lithium thermophysical properties, Fusion Engineering and Design, Vol. 138, 2018, pp. 183-195, DOI: 10.1016/j.fusengdes.2018.11.028

[9] Goodfellow, Metals, Alloys, Compounds, Ceramics, Polymers, Composites. Catalogue 1993/94

[10] F. Maviglia, DEMO PFC Heat Load Specification, EUROfusion, EFDA_D_2NFPNU v1.1, http://idm.euro-fusion.org/?uid=2NFPNU, 2019.

[11] C. Bachmann et al., IDD - Blanket Mechanical Supports, (2019), EFDA IDM Ref. EFDA_D_2NHC86.

[12] A. Tassone, et al., Recent Progress in the WCLL Breeding Blanket Design for the DEMO Fusion Reactor. IEEE Transactions on Plasma Science, 46 (5), pp. 1446-1457, 2018, DOI: 10.1109/TPS.2017.2786046.

[13] G. Bongiovì et al., Multi-Module vs. Single-Module concept: Comparison of thermomechanical performances for the DEMO Water-Cooled Lithium Lead breeding blanket, Fusion Engineering and Design, Vol. 136, 2018, pp. 1472-1478. DOI: 10.1016/j.fusengdes.2018.05.037.